Synaptic and cognitive impairment associated with L444P heterozygous glucocerebrosidase mutation

Wudu Lado,[1,†] Ahrom Ham,[1,†] Hongyu Li,[1,†] Hong Zhang,[2] Audrey Yuen Chang,[1] Sergio Pablo Sardi,[3] Roy N. Alcalay,[1,4] Ottavio Arancio,[2] Serge Przedborsky[1] and Guomei Tang[1]

[†]**These authors contributed equally to this work.**

Abstract

Cognitive impairment is a common but poorly understood non-motor aspect of Parkinson's disease, negatively affecting patient's functional capacity and quality of life. The mechanisms underlying cognitive impairment in Parkinson's disease are still elusive, limiting treatment and prevention strategies.

This study investigates the molecular and cellular basis of cognitive impairment associated with heterozygous mutations in *GBA1*, the strongest risk gene for *Parkinson's* disease that encodes glucocerebrosidase (GCase), a lysosome enzyme that degrades the glycosphingolipid glucosylceramide into glucose and ceramide. Using a *Gba1*$^{L444P/+}$ mouse model, we provide evidence that L444P heterozygous *Gba1* mutation (L444P/+) causes hippocampus-dependent spatial and reference memory deficits independently of α-synuclein (αSyn) accumulation, GCase lipid substrate accumulation, dopaminergic dysfunction and motor deficits. The mutation disrupts hippocampal synaptic plasticity and basal synaptic transmission by reducing the density of hippocampal CA3-CA1 synapses, a mechanism that is dissociated from αSyn-mediated presynaptic neurotransmitter release. Using a well-characterized Thy1-αSyn pre-manifest Parkinson's disease mouse model overexpressing wild type human αSyn, we find that the L444P/+ mutation exacerbates hippocampal synaptic αSyn accumulation, synaptic and cognitive impairment in young *Gba1*$^{L444P/+}$:Thy1-αSyn double mutant animals. With age, Thy1-αSyn mice manifest motor symptoms, and the double mutant mice exhibit more exacerbated synaptic and motor impairment than the Thy1-αSyn mice.

Taken together, our results suggest that heterozygous L444P *GBA1* mutation alone perturbs hippocampal synaptic structure and function, imposing a subclinical pathological burden for cognitive impairment. When co-existing αSyn overexpression is present, heterozygous L444P *GBA1* mutation interacts with αSyn pathology to accelerate Parkinson's disease-related cognitive impairment and motor symptoms.

Author affiliations:

1 Department of Neurology, Columbia University Irving Medical Center, New York, NY10032, USA

2 Department of Pathology and Cell Biology, Columbia University Irving Medical Center, New York, NY10032, USA

3 Rare and Neurologic Diseases Research, Sanofi, Cambridge, MA 02141, USA

4 Movement Disorders Division, Department of Neurology, Tel Aviv Sourasky Medical Center, Tel Aviv 64239, Israel

Correspondence to: Guomei Tang

Department of Neurology, Columbia University Irving Medical Center

630 West 168th street, BB301, New York, NY10032, USA

E-mail: gt2107@cumc.columbia.edu

Running title: Memory deficits associated with GBA1-PD

Keywords: *GBA1*-associated Parkinson's disease; memory deficit; synaptic plasticity; synapse loss, neurodegeneration

Introduction

Parkinson's disease is the most common neurodegenerative movement disorder characterized by tremor, rigidity, and bradykinesia. [1] It is also accompanied by cognitive impairment, including executive dysfunctions and deficits in visuo-spatial working and episodic memory, which often appear in an early, premotor phase of disease, and progressively increase in intensity. [2-5] Current treatments mainly target motor symptoms, leaving therapy for cognitive deficits an unmet clinical need. [6]

Accumulating evidence suggests a strong association between Parkinson's disease and mutations in *GBA1*, [7] the gene that encodes the lysosome enzyme beta-glucocerebrosidase (GCase), which breaks down glucosylceramide (GlcCer) into glucose and ceramide. Homozygous *GBA1* mutations cause Gaucher disease, the most common lysosome storage disorder, [8] whereas heterozygous mutations of *GBA1* confer increased risk for Parkinson's disease. [9] Compared to idiopathic Parkinson's disease patients without *GBA1* mutations (non-*GBA1*-PD), patients carrying heterozygous *GBA1* mutations (*GBA1*-PD) exhibit an earlier age at onset, more severe cognitive impairment, accelerated cognitive decline and higher incidence of dementia. [10, 11]

The mechanism by which *GBA1* mutations increase susceptibility to Parkinson's disease and accelerates the disease progression remains elusive. Given that *GBA1*-PD patients exhibit more diffuse neocortical and hippocampal Lewy body (LB) pathology than non-*GBA1*-PD patients, [12] and that GCase protein is present in ~ 75% of LBs in *GBA1*-PD versus 4% in non-*GBA1*-PD patients, [13] mutations in *GBA1* have been implicated in the development of LB pathology, a feature that is positively correlated with cognitive and motor dysfunction. [12] Consistently, studies have revealed a bidirectional pathogenic interplay between α-synuclein (αSyn) accumulation and GCase deficiency: [14, 15, 16] the loss of GCase enzyme activity causes GlcCer accumulation. The later stabilizes α-Syn oligomers, leading to a further loss of GCase activity. This vicious cycle exacerbates LB pathology, which explains the more rapid progression of motor and non-motor symptoms in *GBA1*-PD. A similar mechanism was proposed for non-*GBA1*-PD, given that GCase protein levels and enzyme activities are reduced in brains of non-*GBA1*-PD patients. [17, 18, 19]

Mutant *Gba1* knockin mice have been generated to model the susceptibility to Parkinson's disease related αSyn pathology and motor symptoms. Among these, heterozygous L444P (L444P/+)

mutant (*Gba1*$^{L444P/+}$) mice are most well-characterized, which carry a severe *Gba1* mutation with ~60% residual GCase activity. [20, 21, 22, 23] The mice exhibit Parkinson's disease-like molecular changes, including impaired autophagy-lysosomal degradation, impaired mitochondrial autophagy, mitochondrial dysfunction, and αSyn accumulation, [20] but no signs of nigrostriatal neurodegeneration and motor dysfunction. [16, 21, 23] The L444P/+ mutation, however, exacerbates motor and gastrointestinal deficits in mice overexpressing human A53T mutant αSyn gene SNCA, [22] and enhances dopaminergic neurodegeneration induced by 1-methyl-4-phenyl-1,2,3,6-tetrahydropyridine (MPTP), [21] AAV-mediated human αSyn overexpression. [23]

Cognitive impairment associated with *GBA1* mutations is less well studied. Here, we show evidence for hippocampus-dependent memory loss in *Gba1*$^{L444P/+}$ mice. The L444P/+ mutation impairs hippocampal synaptic plasticity and basal synaptic transmission by disrupting synaptic structures, an effect that is dissociated from the accumulation of GCase substrates and αSyn, dopaminergic dysfunction and motor deficits. By crossing *Gba1*$^{L444P/+}$ mice to Thy1-αSyn mice overexpressing wild type human αSyn, we generated a *Gba1*$^{L444P/+}$:Thy1-αSyn mouse model. With this double mutant model, we find that the L444P/+ mutation interacts with co-existing αSyn overexpression to exacerbate synaptic and cognitive impairment in young animals, and to augment motor symptoms at older ages. Our study provides first evidence that L444P/+ *Gba1* mutation increases the susceptibility of hippocampal synapse degeneration and cognitive impairment independently of αSyn and lipid accumulation. When αSyn overexpression is present, L444P/+ mutation precipitates αSyn pathology, leading to more severe Parkinson's disease-related cognitive and motor symptoms.

Materials and methods

Mouse Models

Gba1$^{L444P/+}$ mice were from MMRRC (stock number 000117-UNC, B6;129S4 background). *Snca*KO (#003692), *Gba*1$^{flox/flox}$ (#021329), DAT-Cre (#006660) and Cre reporter (#007909) mice were from Jackson Laboratory. Thy1-αSyn mice were a gift from Drs. Eliezer Masliah and Marie-Francoise Chesselet. We crossed *Gba1*$^{L444P/+}$ mice with *Snca*KO mice to obtain Control,

Gba1$^{L444P/+}$, *Snca*+/-, *Snca*KO, *Gba1*$^{L444P/+}$: *Snca*+/- and *Gba1*$^{L444P/+}$: *Snca*KO littermates, and with Thy1-αSyn mice to generate control (CTRL), *Gba1*$^{L444P/+}$, Thy1-αSyn and *Gba1*$^{L444P/+}$:Thy1-αSyn double mutant mice. *Gba1*$^{flox/flox}$ mice were crossed to DAT-Cre mice to generate dopaminergic neuronal specific *Gba1* conditional knockout mice. All mouse procedures were reviewed and approved by Columbia University Medical Center Institutional Animal Care and Use Committee. Mice were maintained under pathogen free conditions under a 12/12 h light/dark cycle, and housed in individually ventilated cages containing cob bedding and environmental enrichment with food and water ad libitum.

Behavioral Analysis

Mice were subjected to behavioral analysis at the ages of 2.5 months and 7 months, using protocols described in Puzzo et al. 2014 [24] and in Wu et al., 2022. [25]

Novel object recognition (NOR)

The mouse was habituated in a translucent arena for 10 min. [25] Twenty-four hours (h) later, the mouse was reintroduced to the arena for 15 minutes, with two identical objects (yellow rubber ducks) placed in opposite corners. After a 30-min break, the mouse was placed back into the arena with one original object and one novel object (yellow cylinder) in the same opposite corners, and video recorded for 15 minutes. After each session of the NOR, the arena and objects were cleaned with 75% ethanol followed by clean water to ensure that behavior of animals was not guided by odor cues. Accumulative time spent sniffing the novel object vs. the original/familiar object was analyzed using Observer XT software (Noldus).

Open field performance

Mice were assessed in an open field arena (27.31 × 27.31×20.32 cm) for 60 minutes. [25] Videos were analyzed with the automated tracking program ANY-Maze (Stoelting). Locomotion activities were determined by measuring total distance traveled (m), anxiety-like behaviors were determined by measuring time in the center (minute) and the number of rearing events.

Contextual and fear conditioning (FC) tests

FC tests were conducted in Plexiglas chambers (Noldus) and recorded using Ethovision XT software. [24, 25] Mice were exposed to the context for 2 min, followed by a conditioning stimulus (CS), e.g., a sound tone (85 dB, 2800 Hz) for 30 s, then by a 0.80 mA foot shock (unconditioned stimulus (US)) for 2 s. After the CS/US pairing, mice were returned to the home cage. Twenty-four hours later, mice were placed back in the same chambers for 5 min to assess contextual fear memory. Another 24 h later, cued fear memory was evaluated in the same chamber with a novel context for 2 min (pre-CS test), after which mice were exposed to the same tone for 3 min (CS test). Freezing response, characterized by lack of movement, was scored automatically by EthoVision software (Noldus). Following FC test, sensory perception of the shock was determined in the same chambers. By increasing the electric current (0.1 mA for 1 s) at 30 s intervals by 0.1 - 0.7 mA, the threshold to flinching (first visible response to shock), jumping (first extreme motor response), and screaming (first vocalized distress) was quantified by averaging of the shock intensity at which each animal manifested a behavioral response of that type to the foot shock.

Two-day radial arm water maze (RAWM) test

Two-day RAWM [24] was performed in a circular pool (120 cm in diameter) filled with opaque water (~24 °C) and equipped with an apparatus consisting of six arms radiating from the center. Spatial cues were present on the walls of the room. A hidden platform was placed at the end of one arm (goal arm), submerged in the water. When needed, the platform was made visible by lifting it up 1 cm above the water and flagged with a yellow bottle cup on the top. Each mouse was tested for 15 trials per day, with the goal arm constant for all trials whereas the starting arms varying on successive trials. Each trial lasted up to 1 minute. At the end of each trial, mice stayed on the platform for 15 s. On day 1, mice were trained to find the platform by alternating between a visible and a hidden platform throughout trials 1 to 12. During the last three trials 13-15, only a hidden platform was used. On day 2, the hidden platform was used throughout 15 trials. Errors were counted when the mice failed to enter the goal arm or select an arm. Data were presented as average errors per block (3 trials per block, 5 blocks per day).

Morris water maze (MMW) spatial learning and reference memory

Following the 2-day RAWM test, the 6-arm apparatus was removed from the pool. The tank was divided into 4 quadrants, with a hidden platform placed in the quadrant 4 (target quadrant). Mice were trained to find the hidden platform for 2 sessions (4 hours apart) per day, each consisting of 4 trials (1 minute each), for 3 days. Time required to reach the hidden platform (escape latency) in the target quadrant was documented. [24] At the end of each trial, mice were guided to the platform and allowed to stay for 20 s. The training was followed by 4 probe trials on day 4, with the platform removed to test the retention of spatial memory. [24] EthoVision (Noldus) video tracking was used to chart the percent of time the animal spent in the target quadrant.

Visible platform test

A visible platform task [24] was applied to assess the visual, motor, and motivation skills of the mice. Mice underwent 3 sets of tests, each consisting of 3 trials in which the mice were trained to find the visible escaping platform. Each trial lasted until the mouse found the platform or until the maximum time of 60 s. Time to reach the platform (latency) and velocity were analyzed using the Ethovision XT video tracking system. The results were shown in 3 blocks and each block represented the average of one set of experiment.

Accelerating Rotarod

Motor coordination and balance were measured using a rotarod at an initial speed of 4 rpm, accelerating up to 40 rpm within 5 minutes. [25] The time (in seconds) taken for a mouse to fall from the rod was measured. Mice were trained for 3 days, three trials per day (inter-training interval, 30 min), and tested with three trials on day 4.

Balance Beam walking

The apparatus consists of 1-meter beam with a flat surface of 12 mm resting 50 cm above the table top. A black box was placed at the end of the beam as the finish point. A lamp was above the start point and the light served as an aversive stimulus. Mice were placed at the start point of the beam and the time to cross the beam was documented.

Western Blotting Analysis

Mice were sacrificed by cervical dislocation. Hippocampal protein lysates were prepared and subjected to Western blotting analysis, as in Wu et al., 2022. [25] Triton X-100 (Sigma, T9204)-soluble and -insoluble αSyn protein was assessed as described in Rockenstein et al., 2014 [26] and Li et al., 2019. [20] Blots were imaged using the Bio-Rad ChemiDoc™ Touch Imaging System. The optical densities of protein bands were quantified using Image J, and data were expressed as percentage (%) of control mean and presented as mean ± SEM. Four mice per genotype were used at each age. Primary antibodies were: synapsin I, anti-Rabbit, Millipore #AB1543; synaptophysin, anti-mouse, Abcam #ab8049; GBA, anti-Rabbit, Sigma #G4171; αSyn, anti-Rabbit, Sigma #S3062; PSD95, anti-Rabbit, Abcam #ab18258; PSD95, anti-mouse, Millipore #MAB1596; p-αSyn Ser129, anti-mouse, WAKO #015-25191; actin, anti-mouse, Sigma #A5441; NeuN, anti-rabbit, Cell signaling technology, #24307; Lamin B, anti-rabbit, Abcam #ab116048; GluR1, anti-mouse, NeuroMab #75-327; GAPDH, anti-rabbit, Proteintech, #10494-1-AP. All data were generated from experiments with at least 3 replicates.

Crude Synaptosome Fractionation

Crude synaptosome was fractionated according to Wirths, 2017. [27] Hippocampal tissue was homogenized in cold buffer 5 mM HEPES, pH 7.5, 0.32M sucrose supplemented with protease and phosphatase inhibitors. Homogenates were cleared at 1000 g for 10 min to remove nuclei and large debris (P1 fraction). The resulting supernatants were concentrated at 12,000 g for 20 min to obtain the pellet fraction (P2), which was resuspended in 5 mM HEPES, 1 mM EDTA, pH 7.4 to pellet the crude synaptosome fraction (20 min at 12,000 g). Proteins were extracted from total homogenates, the nuclear fraction, the cytosolic and the synaptosome fractions and subjected to Western blot analysis, as in Wu et al., 2022 [25].

Immunohistochemistry and DiOlistic Labeling

Mice were anesthetized with isoflurane and perfused with 4 % paraformaldehyde (PFA)(w/v) in 0.1M PBS (PH7.4). For Immunohistochemistry (IHC), brains were removed and post-fixed in 4% PFA at 4°C overnight. 30 μm thick coronal sections were prepared using a Leica VT1000S

vibratome, and subjected to IHC, as described in Wu et al., 2022. [25] Experiments without primary antibodies were conducted to control for the specificity of each primary antibody. For all experiments, 3 mice were used for each genotype/condition, and 3-5 coronal sections containing hippocampus were used from each mouse.

DiOlistic labeling was conducted in 200 µm thick slices prepared immediately following perfusion fixation, according to Wu et al., 2022. [25] Hippocampal slices were labeled with DiI (Thermofisher Scientific, #D282) using a Helios gene gun system at 120 pounds per square inch (psi). Segments of basal and apical dendrites 100-200 µm distant from the soma were imaged with a Leica multiphoton system. Twenty DiI- labeled CA1 pyramidal neurons were randomly chosen from 3 mice and 3-4 dendritic segments per neuron were imaged. Z-stack images (pixel size 1024 X 1024, image size 42 X 42 µm, step size 0.2 µm) of dendritic segments were reconstructed using Imaris software (Bitplane) for spine analysis. Mature mushroom spines were defined as dendritic protrusions with head/neck diameter ratio 1.1. [25] For the analysis of dendrites, confocal image stacks (pixel size 1024 X 1024, image size 295X295 µm, step size 0.3 µm) were acquired. Merged images were subjected to sholl analysis using Image J, as described in Wu et al., 2022. [25]

Slice Physiology

Acute brain slices were prepared as in Wu et al., 2022. [25] Slices were recovered in artificial CSF (aCSF, in mM: 125 NaCl, 2.5 KCl, 26 $NaHCO_3$, 1.25 NaH_2PO_4, 2 $CaCl_2$, 1.5 $MgCl_2$, 10 D-glucose). Following recovery, slices were transferred to a recording chamber and perfused with oxygenated aCSF (3 ml/min) at 32°C. Cells were patched using a glass pipette (tip resistance, 3-5 mΩ) filled with intracellular pipette solution (in mM): 130 K-gluconate, 10 KCl, 10 HEPES, 0.2 EGTA, 0.3 $CaCl_2$,1 $MgCl_2$, 3 Mg-ATP, 0.3 Na-GTP (pH 7.3 with KOH). We measured **(1)** miniature excitatory postsynaptic currents (EPSCs) by holding membrane potential at -70 mV using pCLAMP 8.2.0.235 and MultiClamp 700A commander (version 1.3.0.05) in presence of 1 µM TTX (Tocris, #1069); **(2)** evoked EPSCs, by placing a tungsten concentric bipolar microelectrode (World Precision Instruments, Inc., USA) at Schaffer collateral. Extracellular stimulation (0.2 ms duration, 200 µA current intensity) was applied using an Isostim™ A320 Stimulus isolation unit (World Precision Instruments, Inc., USA). The peak of AMPAR-mediated EPSCs was measured by holding membrane potential at -70 mV, and the peak of NMDAR-

mediated EPSCs was determined at +40 mV, 50 ms from the stimulus artifact. The AMPAR/NMDAR receptor ratio was calculated by dividing the amplitude of the AMPAR current by the NMDAR current; **(3)** paired pulse facilitation in CA1 pyramidal neurons, elicited by two Schaffer collateral stimuli delivered at the interstimulus interval 50 ms. Paired pulse ratio was defined by the ratio of EPSC amplitude in response to the second versus the first stimulus (P2/P1). For LTP recording, a 20-min baseline of field excitatory postsynaptic potentials (fEPSPs) was recorded every minute at an intensity that evokes a response ~35% of the maximum evoked response. LTP was induced using θ-burst stimulation (TBS, 4 pulses at 100 Hz, with the bursts repeated at 5 Hz and each tetanus including three 10-burst trains separated by 15 s). Responses were recorded for 90 minutes after TBS and measured as fEPSP slope expressed as percentage of baseline.

Gcase Enzyme Activity

GCase enzyme activity was measured in lysosome-enriched fractions using 4-methylumbelliferyl β-D-glucopyranoside (Sigma, M3633) as a substrate, as in Li et al., 2019. [20] All data were acquired from experiments with 4 replicates.

Lipid Extraction and Mass Spectrometry

Lipid Extraction was performed as described previously. [28, 29, 30] The lipid extract was spiked with appropriate internal standards, and analyzed using the Agilent 1260 HPLC system coupled to an Agilent 6490 Triple Quadrupole mass spectrometer (Agilent Technologies, Santa Clara, CA). GluCers (GluCer d18:1/16:0, d18:1/18:0, d18:1/22:0, d18:1/24:0, d18:1/24:1, Avanti) and GluSph (GluSph 18:1) were quantified using GluCer d18:1 and GlcSph d18:1 standards (Avanti), as in Sardi et al., 2011. [28] Total GlcCer was represented as the sum concentrations of C16:0 through C24:1 chain length variants. Lipid concentration was expressed as ng/mg of tissue sample. [28] Lipidomic profiles for other lipid classes were quantified according to Clark et al., 2015 [29] and Surface et al., 2022, [30] using multiple reaction monitoring (MRM) transitions developed by Chang et al., 2012 [31] and by referencing to the signal intensities of known quantities of internal standards: PA 14:0/14:0, PC 14:0/14:0, PE 14:0/14:0, PG 15:0/15:0, PI 12:0/13:0, PS 14:0/14:0, BMP 14:0/14:0, APG 14:0/14:0/14:0, LPC 13:0, LPE 14:0, LPI 13:0, Cer d18:1/17:0, SM d18:1/12:0,

dhSM d18:0/12:0, GalCer d18:1/12:0, Sulf d18:1/12:0, LacCer d18:1/12:0, CE 17:0, MG 17:0, DG, TG 16:0/18:0/16:0 and Lipidomix HP(25) (Avanti Polar Lipids, Alabaster, AL). GM3 and globotriaosylceramide (Gb3) lipid species were referenced to the internal standards that were closest to it in the elution gradient. Mol% values were calculated by dividing individual lipid concentration by the total lipid concentration of each sample.

Statistical Analysis

Sample sizes of all mouse experiments were determined based on the relevant published literature in the field. Both genders were considered unless specified. Mice were coded and randomly assigned to each experiment, and all investigators were blinded to group allocation and genotypes during data acquisition and analysis. Statistical analyses were performed using Graphpad Prism software. We used Kolmogorov-Smirnov and D'Agostino-Pearson normality tests to determine data normality, and F-test to compare variance between groups. Differences between two groups were analyzed by two-tailed unpaired t-test (normal distribution and equal variance), Welch's *t*-test (normal distribution and unequal variance) or Mann–Whitney test (non-normal distribution). Multiple group comparisons were conducted by one-way or two-way ANOVA followed by Tukey's multiple comparisons test or Fisher's least significant difference (LSD) test. All data were presented as mean ± SEM. The level of significance was set at $p < 0.05$.

Results

Gba1$^{L444P/+}$ mice exhibit cognitive impairment without motor involvement

Using the fear conditioning (FC) test, we assessed the ability of *Gba1*$^{L444P/+}$ mice to learn and memorize an association between an aversive stimulus, i.e., an electrical foot shock, and complex stimuli such as context (e.g., a new environment) or cues (e.g., a tone). This learning paradigm relies on the hippocampus and amygdala, with the hippocampus indispensable for contextual learning, whereas the amygdala involved in cued conditioning. [24] Compared to wild type (WT) control littermates (CTRL), *Gba1*$^{L444P/+}$ mice showed impairments in contextual but not cued memory at 7 months of age (**Fig. 1A**). Our data corroborate a recent report of reduced

contextual memory in *Gba1*$^{L444P/+}$ mice at 3 months of age. [32] Further assessment of the sensory threshold revealed no between-group difference (**Fig. 1B**), suggesting that L444P/+ mutation does not affect perception of the electric shock. These data indicate that *Gba1*$^{L444P/+}$ mice have a selective hippocampus-dependent impairment in associative learning and memory.

Hippocampus dependent working memory was assessed in a radial arm water maze (RAWM). [24] At 7 months, compared to CTRL, *Gba1*$^{L444P/+}$ mice showed increased number of failures to reach the hidden platform during the test session, suggesting impairments in short-term spatial working memory (**Fig.1C**). Spatial reference memory was assessed in a hidden platform Morris water maze (MWM). [24] Both CTRL and *Gba1*$^{L444P/+}$ mice performed equally well in spatial learning and showed a progressive reduction in the time to locate the hidden platform during the training session (**Fig. 1D**). In the probe test, *Gba1*$^{L444P/+}$ mice spent significantly less time in the target quadrant than CTRL littermates (**Fig. 1E**), suggesting impairments in spatial memory. Using a visible platform test, we excluded the presence of sensory deficits that may prevent the mice from identifying visual cues, given that all CTRL and *Gba1*$^{L444P/+}$ mice reached the visible platform with similar time and swimming speed (**Fig. 1 F-G**).

We next examined novel object recognition (NOR) memory, a declarative memory that mice make use of their innate preference for novel over familiar objects. [33] At 7 months, CTRL mice preferred to sniff the novel object more than the familiar one **(Fig. 1H**), whereas *Gba1*$^{L444P/+}$ mice spent less time exploring the novel object, with impaired preferences for the novel object.

To control for locomotor activity, mice were subjected to open field test and recorded for total distance traveled, frequency for rearing and the time spent in center. Motor learning and coordination were assessed using the accelerating rotarod and balance beam tests. No impairments in rotarod, balance beam and open field performances were found in *Gba1*$^{L444P/+}$ mice at 7 months (**Fig. 1 I, J, K**). Therefore, memory loss in *Gba1*$^{L444P/+}$ mice should result from defects in cognition but not altered visual ability, sensory, motility or motivation.

By dividing the mice into male and female subgroups, we found that both male and female *Gba1*$^{L444P/+}$ mice showed memory deficits with intact motor function relative to their same-sex control littermates (**Supplementary Fig. 1**). Behavioral tests, including FC, MWM, rotarod and open field tests, were administered in separate cohorts of male and female *Gba1*$^{L444P/+}$ mice at a younger age of 2.5 months. Both male and female *Gba1*$^{L444P/+}$ mice showed comparable

impairments in FC contextual memory and MWM spatial reference memory, with no defects in motor functions (**Supplementary Fig. 2**). Together, our data suggest that *Gba1*$^{L444P/+}$ mice do not show age and gender differences in their cognitive phenotypes, and that the presence of the heterozygous *Gba1* mutation per se is sufficient to cause cognitive dysfunction without motor involvement.

Impaired hippocampal synaptic plasticity and basal synaptic transmission in *Gba1*$^{L444P/+}$ mice

To assess the effect of *GBA1* mutation on synaptic function that may account for hippocampus-dependent cognitive deficits, we recorded hippocampal CA3-CA1 long term potentiation (LTP), a well-known electrophysiological surrogate of hippocampus-dependent learning and memory. [34] Compared to CTRL, *Gba1*$^{L444P/+}$ mice showed impaired LTP at the age of 2.5 months (**Fig. 2A**).

We next measured spontaneous activities of hippocampal CA3-CA1 synapses by recording miniature excitatory postsynaptic currents (mEPSCs) in CA1 pyramidal neurons. Compared to CTRL, *Gba1*$^{L444P/+}$ neurons showed a significant reduction in mEPSC frequency at 2.5 months (**Fig. 2B**). Decreased mEPSC frequency is conventionally interpreted to suggest a presynaptic inhibition or a reduction in functional synaptic density. To test this possibility, we examined paired pulse facilitation (PPF), a form of short-term synaptic plasticity that is used to infer the changes in the probability of presynaptic release, in which the response of the second of two consecutive stimuli with a given interstimulus interval (ISI) is higher than the first one. As in **Fig. 2C**, we did not find between-group differences in PPF, suggesting normal presynaptic release in *Gba1*$^{L444P/+}$ mice. Morphological analysis however revealed a reduction in basal dendritic tree complexity and the density of mature dendritic spines of CA1 pyramidal neurons in *Gba1*$^{L444P/+}$ mice (**Fig.2 D and E**), indicative of a loss of functional excitatory synapses. The synapse loss was confirmed by Western blot analysis of pre- and post-synaptic markers (**Fig. 2F**), demonstrated by a reduction in levels of presynaptic proteins, e.g., synapsin I (SYN1) and synaptophysin (SYP), and postsynaptic protein PSD95. The levels of the neuronal marker NeuN remained unaltered in the hippocampus of *Gba1*$^{L444P/+}$ mice (**Fig. 2F**). This result coincides with our previous report of normal cell survival in *Gba1*$^{L444P/+}$ hippocampal neurons *in vitro* in cultures, [20] supporting a lack of hippocampal neuronal loss in *Gba1*$^{L444P/+}$ mice. Together, our data indicate that basal synaptic transmission is

impaired in *Gba1*$^{L444P/+}$ mice due to a loss of excitatory synapses.

Depletion of αSyn fails to rescue synaptic and cognitive impairments in *Gba1*$^{L444P/+}$ mice

We then asked whether αSyn accumulation accounts for the synaptic and cognitive impairment *in vivo* in *Gba1*$^{L444P/+}$ mice. We downregulated αSyn levels genetically using the αSyn gene (*Snca)* knockout (KO) mice (**Fig**. **3A**). Control, *Gba1*$^{L444P/+}$, *Snca*+/-, *Snca*KO, *Gba1*$^{L444P/+}$: *Snca*+/- and *Gba1*$^{L444P/+}$: *Snca*KO littermates were subjected to FC, MWM, accelerating rotarod and open field tests at 2.5 months. Neither *Snca*+/- or *Snca*KO mice showed cognitive and motor impairment, and the depletion of one or two copies of *Snca* alleles had no effect on learning and memory deficits in *Gba1*$^{L444P/+}$ mice (**Fig**. **3 B-G**).

By comparing electrophysiological properties of hippocampal CA3-CA1 synapses among control, *Gba1*$^{L444P/+}$, *Snca*KO, and *Gba1*$^{L444P/+}$:*Snca*KO littermates at 2.5 months, we asked whether L444P/+ mutation interferes with hippocampal synaptic transmission through αSyn accumulation. Consistent with previously reported intact hippocampal synaptic plasticity in *Snca*KO mice, [35] we found that the loss of αSyn had no effects on basal synaptic transmission, including mEPSC (**Fig**. **3H**) and PPF (**Fig**. **3I**). Similar to *Gba1*$^{L444P/+}$ littermates, *Gba1*$^{L444P/+}$:*Snca*KO mice showed a reduction in mEPSC frequency (**Fig**. **3H**) but no changes in PPF (**Fig**. **3I**). Thus, the effects of mutant GCase on hippocampal synaptic and cognitive impairment at young ages are not associated with αSyn accumulation.

Age-dependent manifestation of lipid changes in *Gba1*$^{L444P/+}$ mice

A prevailing hypothesis for GBA-PD is that the loss of GCase enzyme activity alters lipid composition, resulting in αSyn pathology. [15, 16] To test this loss of function hypothesis *in vivo*, we measured GCase enzyme activity and the levels of GCase lipid substrates glucosylceramide (GluCer), as well as the deacetylated form of GluCer, glucosylsphingosine (GluSph). Despite a reduction in GCase enzyme activity (**Fig**. **4 A, B**), *Gba1*$^{L444P/+}$ mice showed no evidence for hippocampal GluCer accumulation at 2.5 and 7 months of age. Levels of hippocampal GluSph remained unaltered at 2.5 months but were increased at 7 months (**Fig**. **4 C, D**). Our data are consistent with Mahoney-Crane et al [32] findings in the forebrain of *Gba1*$^{L444P/+}$ mice, confirming a lack of GCase substrate accumulation at the age when cognitive deficits began to manifest.

Lipidomic analysis of other lipid classes, including cholesterols, phospholipids, lysophospholipids, sphingolipids and gangliosides, showed no changes in *Gba1*$^{L444P/+}$ mice at 2.5 months (**Fig. 4 E**). These data suggest that synaptic and cognitive impairment in *Gba1*$^{L444P/+}$ mice may emerge at 2.5 months in the absence of gross lipid alterations.

Gba1$^{L444P/+}$ mice, however, presented profound lipid changes at 7 months of age (**Fig. 4 F**), including an increase in sterols and glycerol lipid classes, e.g., free cholesterol (FC), cholesterol esters (CE) and diacylglycerol (DAG), and a reduction in the most abundant *phospholipids*, including phosphophatic acids (PA), phosphatidylethanolamine (PE), plasmalogen phosphatidyl-ethanolamine (PEp), phosphatidylserine (PS) and phosphatidylinositol (PI). Consistently, the levels of lyso-forms of phospholipids (lysophospholipids), including lysophosphatidylcholine (LPC) and lysophosphatidylserine (LPS), and the endo-lysosomal phospholipid bis(monoacylglycero)phosphate (BMP), a metabolite downstream of Lysophosphatidylglycerol (LPG), were downregulated *in Gba1*$^{L444P/+}$ mice. The mutants also exhibited an increase in the ganglioside GM3 and a reduction in the sphingolipid ceramide.

L444P/+ *Gba1* mutation exacerbates synaptic and cognitive impairment in Thy1-αSyn mice at 2.5 months

To further assess the relevance of L444/+ *GBA1* mutation in Parkinson's disease -related cognitive and motor impairment, we used a well-characterized transgenic mouse model that overexpresses WT human αSyn under the murine Thy1 promoter (Thy1-αSyn, line 61). This model exhibits several motor and nonmotor features of idiopathic Parkinson's disease with age. [36, 37] Notably, the mice develop αSyn aggregates in both nigrostriatal and neocortical-limbic systems at young ages, but undergo a progressive loss of striatal dopamine and dopaminergic synaptic terminals until after 14 months. [36, 37] The modest overexpression of human αSyn does not suppress brain GCase enzyme activity, [26] providing a means to investigate the effects of both *GBA1* mutation and pre-existing αSyn pathology on Parkinson's symptom. [38, 39]

By crossing *Gba1*$^{L444P/+}$ and Thy1-αSyn mice, we generated *Gba1*$^{L444P/+}$:Thy1-αSyn double mutant mice. To monitor the progress of disease phenotypes, we assessed cognitive and motor functions in control (CTRL), *Gba1*$^{L444P/+}$, Thy1-αSyn and the double mutant littermates at ages of 2.5 and 7 months. Because the Thy1-αSyn transgene is located in the X chromosome, which may cause

random inactivation in somatic cells in female mice, [36] we only included male mice for this experiment.

At 2.5 months, both *Gba1*$^{L444P/+}$ and Thy1-αSyn mice showed similar levels of impairments in contextual (**Fig. 5A**) and MWM spatial reference memory (**Fig. 5C**), with no signs of motor deficits (**Fig. 5D, E**), except that the Thy1-αSyn mice presented a slower MWM learning process relative to the *Gba1*$^{L444P/+}$ littermates (**Fig. 5B**). Compared to Thy1-αSyn littermates, the double mutants displayed a further decline in contextual memory (**Fig. 5A**), MWM spatial learning (**Fig. 5B**) and memory (**Fig. 5C**), but no changes in motor function (**Fig. 5D, E**).

Consistently, both *Gba1*$^{L444P/+}$ and Thy1-αSyn mice showed impaired hippocampal LTP, whereas the double mutants presented more exacerbated LTP impairment than both single mutant lines (**Fig. 5F**). At synapse level, *Gba1*$^{L444P/+}$ littermates continued to show reduced mEPSC frequency (**Fig. 5G**) with no changes in presynaptic release (**Fig. 5H**). Thy1-αSyn littermates, however, presented a reduction in mEPSC frequency (**Fig. 5G**) that was associated with an increase in pair pulse ratio (PPR) (**Fig. 5H**), which corroborates previously reported presynaptic inhibition by αSyn overexpression. [40, 41] Compared to Thy1-αSyn littermates, the double mutants showed a further reduction in mEPSC frequency (**Fig. 5G**) but no additional changes in pair pulse ratio (**Fig. 5H**). All three mutant lines showed similar evoked NMDA- and AMPA- receptor responses relative to CTRL littermates (**Fig. 5 I**), suggesting that both L444P/+ mutation and αSyn overexpression have subtle postsynaptic effects at 2.5 months. Together, our results suggest different synaptic mechanisms of *GBA1* mutation and αSyn overexpression: while αSyn overexpression affects presynaptic neurotransmitter release, [40, 41] L444P/+ mutation inhibits synaptic transmission by reducing the number of synapses.

We confirmed this difference by Western blot analysis of pre- and postsynaptic proteins synapsin 1 (SYN1) and PSD95 (**Fig. 6A**): *Gba1*$^{L444P/+}$ mice showed a reduction in both SYN1 and PSD95, whereas Thy1- αSyn mice only exhibited a decrease in SYN1 but not PSD95 levels. It is likely that an additive effect may exist between L444P/+ mutation and co-existing αSyn overexpression, resulting in more reduced mEPSC frequency in the double mutants at this young age.

Using Western blot (**Fig. 6A**) and immunohistochemistry (**Fig. 6B**), we examined protein levels of total αSyn and Ser129 phosphorylated αSyn (p-αSyn), a species that is abundant in αSyn lesions in diseased human brain [42] and in transgenic mice overexpressing WT mouse or human αSyn, [26, 43]

Compared to CTRL littermates, *Gba1*$^{L444P/+}$ mice showed higher levels of total αSyn but no obvious changes in p-αSyn, whereas Thy1-αSyn mice displayed a significant increase in both total αSyn and p-αSyn. The double mutants showed a further accumulation of both total αSyn and p-αSyn compared to the Thy1-αSyn littermates (**Fig. 6A, B**).

Consistent with Rockenstein et al findings, [26] we observed hippocampal αSyn puncta in Thy1-αSyn mice. These puncta were positive for synaptic marker synaptophsyin (SYP), supporting a synaptic accumulation of αSyn (**Fig. 6C**). Compared to Thy1-αSyn littermates, the double mutants showed more hippocampal αSyn puncta (**Fig. 6D**), suggesting that the L444P/+ mutation exacerbates synaptic αSyn accumulation, an effect that was confirmed by Western blot analysis of αSyn and p-αSyn in synaptosomes purified from Thy1-αSyn mice and the double mutants (**Fig. 6E, F, G, H**). Again, *Gba1*$^{L444P/+}$ mice showed a slight accumulation of αSyn but not p-αSyn. Compared to Thy1-αSyn littermates, the double mutants exhibited a further accumulation of synaptosomal αSyn and p-αSyn (**Fig. 6G, H**). Of note, at this young age, GCase enzyme activity was decreased by ~40% in both *Gba1*$^{L444P/+}$ mice and the double mutants (**Fig. 6 I**), but the levels of GCase substrates, GluCer and GluSph, remained unaltered in all mutant mice (**Fig. 6J**).

L444P/+ *Gba1* mutation exacerbates motor symptoms and αSyn pathology in Thy1-αSyn mice at 7 months

At 7 months, Thy1-αSyn mice showed more severe cognitive impairment accompanied by compromised motor function (**Fig. 7 A-E**). Compared to Thy1-αSyn littermates, the double mutants presented similar levels of impairments in contextual memory (**Fig. 7A**), MWM spatial learning and memory (**Fig. 7B, C**), but more severe rotarod motor deficits (**Fig. 7E**), suggesting that the L444P/+ mutation may augment motor symptoms induced by αSyn overexpression. At the synapse level, both Thy1-αSyn mice and the double mutants showed more compromised LTP than *Gba1*$^{L444P/+}$ littermates (**Fig. 7F**), but the presence of L444P/+ mutation failed to further exacerbate LTP deficits in the double mutants.

It could be that there is a ceiling effect of αSyn pathology and synaptic deficits so that the presence of L444P/+ mutation no longer intensifies cognitive impairment in the double mutants at 7 months of age. Compared to Thy1-αSyn littermates, the double mutants showed similar levels of

hippocampal total αSyn but displayed higher levels of p-αSyn and a further reduction in levels of GCase and synaptic proteins (PSD95, SYN1) (**Fig. 7G**). The greater increase in p-αSyn levels in the double mutants was consistent with a further accumulation of Triton X-100 insoluble αSyn oligomers (**Supplementary Fig. 3**). At this older age, GCase enzyme activity was reduced by ~55% in *Gba1*$^{L444P/+}$ mice and ~62% in the double mutants (**Fig. 7H**), and both *Gba1*$^{L444P/+}$ and double mutant mice showed an accumulation of GluSph (**Fig. 7I**).

L444P/+ *Gba1* mutation causes cognitive impairment independently of dopaminergic dysfunction

Lastly, we asked whether *GBA1* L444P/+ mutation contributes to cognitive impairment by disrupting dopaminergic function. We restricted our analysis at 2.5 months of age when cognitive impairment developed in both *Gba1*$^{L444P/+}$ and Thy1-αSyn mice in the absence of motor signs. Using reverse phase HPLC, we did not find changes in extracellular DA and DOPAC concentration in different brain regions of *Gba1*$^{L444P/+}$ mice, including hippocampus, prefrontal cortex, striatum and midbrain (**Fig. 8A**). Neither did Thy1-αSyn mice or the double mutants show changes in DA and DOPAC levels (**Fig. 8A**). Our data are consistent with Yun et al [21] study in *Gba1*$^{L444P/+}$ mice or Chesselet et al [36] work in young Thy1-αSyn mice, both showed a lack of loss of SNpc DA neurons or striatal TH positive fiber density at young ages.

By crossing *Gba1*$^{flox/flox}$ mice to the DAT promoter driven Cre (DAT-Cre) mice, we generated a dopaminergic neuronal specific *Gba1* conditional knockout (CKO) mouse model. We found that both cognitive and motor functions were well preserved in either *Gba1*$^{flox/+}$:DAT-Cre heterozygous (*Gba1*Het) or *Gba1*$^{flox/flox}$:DAT-Cre+ homozygous (*Gba1*CKO) CKO mice (**Fig. 8 B-H**). Our data corroborate Soria et al [43] findings of normal motor performance and persevered dopaminergic neurons in *Gba1CKO* mice, suggesting that loss of *Gba1* in mouse dopaminergic neurons is not critical for the initiation of cognitive impairment at young ages.

Discussion

Cognitive impairment is a common and disabling non-motor aspect of Parkinson's disease, negatively impacting patients' functional capacity and quality of life. The goal of this study is to

understand the pathogenic mechanisms of cognitive impairment associated with *GBA1* mutations, the strongest genetic risk factor for Parkinson's disease. We provide evidence for impaired hippocampus-dependent short-term working memory, long-term spatial memory and recognition memory in *Gba1*$^{L444P/+}$ mice. Our findings corroborate recent clinical observations of memory deficits in *GBA1* carriers without Parkinson's disease, [45, 46, 47] suggesting a potential mechanism of L444P/+ *GBA1* mutation in hippocampal pathology that is a clear candidate for cognitive impairment.

The hippocampus is a key structure for the formation of spatial and episodic memories. [48] Both structural and functional abnormalities of hippocampus have been reported in Parkinson's disease, and positively correlate with deficits in learning and long-term recall. [49, 50, 51] Consistently, we find a reduction in dendritic complexity, synapse loss together with Parkinson's disease-related molecular changes [20] in the hippocampus of *Gba1*$^{L444P/+}$ mice. The mice do not show motor deficits or changes in DA levels, suggesting that cognitive impairment associated with L444P *GBA1* mutation may occur independently of, or prior to, dopaminergic dysfunction.

We unexpectedly find that downregulating αSyn was unable to mitigate the effects of *GBA1* mutation on synaptic and cognitive function, suggesting that *GBA1* mutation may trigger cognitive deficits independently of αSyn accumulation. It is likely that in *Gba1*$^{L444P/+}$ mice, elevated levels of endogenous αSyn have not reached a threshold level to accumulate αSyn species that mediate early synapse pathology in Parkinson's disease, including oligomeric and aggregated αSyn. [26] Supporting this hypothesis, we find that *Gba1*$^{L444P/+}$ mice do not accumulate p-αSyn (**Fig. 7G**) and αSyn oligomers (**Supplementary Fig. 3**), consistent with previous reports that these mice are unable to develop proteinase K-resistant αSyn aggregates. [21, 23]

GBA1-PD research over the past decade has focused on the loss of GCase enzyme activity and the resulting lipid substrate accumulation as a mechanism for the development of symptoms of Parkinson's disease. We however find no changes in GCase lipid substrates or any other lipid classes in *Gba1*$^{L444P/+}$ mice at 2.5 months when cognitive deficits manifest. It is possible that the mutation-associated reduction in GCase enzyme activity (~40% at 2.5 months) is not sufficient to cause lipid substrate accumulation. Nevertheless, a lack of GCase substrate accumulation has been reported in brains of Parkinson's disease patients with or without *GBA1* mutation, [52] and in D409V/+, L444P/+ and N370S/+ *Gba1* knockin or *Gba1*+/- hemizygous knockout mice. [16, 28]

Moreover, *Gba1* haploinsufficiency was found unable to cause cognitive impairment, [28, 53, 54] and a recent MOVES-PD clinical trial failed to support the GCase substrate accumulation hypothesis. [55]

This leaves an important question open, i.e., how Parkinson's disease-associated heterozygous *GBA1* mutations, e.g., L444P and N370S, result in cognitive impairment in the absence of gross lipid substrate accumulation and αSyn aggregation. *GBA1* mutations can produce ER stress and autophagy-lysosome dysfunction, both can impair protein homeostasis in dopamine neurons, leading to their vulnerability in Parkinson's disease. [56, 57] Additional mechanisms may involve mitochondrial dysfunction due to impaired mitochondrial autophagy [20] or a recently identified interaction between mutant GCase and mitochondrial complex I. [58] These alternative mechanisms highlight the early pathogenic relevance of *GBA1* mutation in synapse degeneration, and may explain the higher risk for *GBA1*-mutation carriers to develop cognitive impairment.

At 7 months, *Gba1*$^{L444P/+}$ mice showed a further reduction (~55%) in GCase enzyme activity that was accompanied by an accumulation of GluSph, a reduction in phospholipids and ceramide (Cer), an accumulation of cholesterol and the ganglioside GM3. These lipid changes are consistent with previous reports in postmortem brains (e.g., reduced PE, BMP and Cer, and elevated GM3), CSF (e.g., elevated GM3) or blood samples (e.g., reduced PE and elevated GM3) from patients with Parkinson's disease, [29, 59-66] and are found to disrupt synaptic transmission and plasticity that underlie cognitive performance [60] or facilitate αSyn aggregation. [67, 68] Consistently, we find that compared to Thy1-αSyn mice, the double mutants present a further increase in p- αSyn and Triton X-100 insoluble αSyn oligomers at 7 months of age. It is likely that the age-dependent decline in GCase function and lipid changes may exacerbate synaptic and cognitive decline in *GBA1*-PD, either by facilitating disease-associated αSyn oligomerization or by further disrupting synaptic structures.

Given that heterozygous *GBA1* mutations do not always result in Parkinson's disease but simply raise the relative risk for the disease, and that *GBA1* mutations only present in 5-20% of patients, [5, 6, 7] a concern remains as to whether cognitive phenotypes in *Gba1*$^{L444P/+}$ mice are relevant to Parkinson's disease. Our findings suggest that L444P/+ mutation per se may confer a subclinical disease burden for cognitive impairment among non-manifesting carriers, and accelerate cognitive decline in patients with Parkinson's disease. *GBA1* mutation carriers will have to be

exposed to additional Parkinson's risk factors, e.g., genetic mutations, aging or oxidative damages, and *GBA1* mutation interacts with these risk factors to trigger Parkinson's disease-related motor symptoms. Without a second insult, pathological changes in *GBA1* carriers may not exceed a threshold to induce Parkinsonism. Supporting this hypothesis, we find that heterozygous L444P/+ mutation exacerbates synaptic and cognitive impairment in young Thy1-αSyn mice, and precipitates motor symptoms at an older age.

In summary, our study provides first evidence for synaptic and cognitive impairments associated with heterozygous L444P *GBA1* mutation that are independent of the accumulation of αSyn and GCase lipid substrates. *Gba1*$^{L444P/+}$ mice may represent a model of mild cognitive impairment that features variable impairments in visual-spatial memory capacities without Parkinsonian motor deficits. In contrast, the *Gba1*$^{L444P/+}$:Thy1-αSyn double mutant mice with pre-existing αSyn accumulation can better reflect clinical representation of Parkinson's disease, showing mild cognitive impairment in advance of parkinsonian motor signs. Using this double mutant model, we show evidence that heterozygous *Gba1* mutation exacerbates synaptic and cognitive impairment in young animals by interacting with co-existing αSyn accumulation, largely through an additive effect of *Gba1* mutation mediated synapse loss and αSyn-mediated presynaptic inhibition. The added impact of aging further reduces hippocampal GCase enzyme activity, leading to a late-age manifestation of lipid changes at 7 months. It is likely that, with age, an expected detrimental association between lipid changes (e.g., elevated GluSph and GM3) and αSyn aggregation may promote spreading of αSyn pathology *in vivo*, leading to increased susceptibility of dopaminergic neuronal loss and accelerated cognitive decline and motor symptoms. Further studies are needed to test these possibilities, and to uncover the implication of *GBA1* mutation in other pathological features of Parkinson's disease, e.g., neuroinflammation. Additionally, various *GBA1* mutations may reduce GCase enzyme activity to a different extent, and various brain cells may respond to *GBA1* mutation differently. [69] Thus, future research will be necessary to assess the mutation- or cell type specific impact of *GBA1* mutations on Parkinson's disease -related features.

Data availability

Source data are provided in Supplementary tables, and will be available from the corresponding author upon request.

Acknowledgements

G.T. and O.A. designed the project. A.H., H. L. and G.T. conducted mouse breeding, genotyping and behavioral analysis; A.H., A.Y.C. and GT performed histological and biochemical analysis; W.L. and H.Z. worked on electrophysiology; G.T., O.A., S.P., R. A. and S.P. wrote the paper. All authors provided critical feedback and helped shape the research, analysis and manuscript. We thank Drs. Eliezer Masliah and Marie-Francoise Chesselet for providing us the Thy1-αSyn mouse model. We also thank Dr. Xiaoping Wu for his technical advice on slice physiology.

Funding

This project was funded by NIH/NINDS R01 NS104390 and Parkinson disease foundation.

Competing interests

The authors report no competing interests.

Supplementary material

Supplementary material is available at *Brain* online.

References

1. Braak H, Del Tredici K, Rüb U, de Vos RA, Jansen Steur EN, Braak E. Staging of brain pathology related to sporadic parkinson's disease. *Neurobiol Aging*. 2003; 24: 197-211.
2. Laatu S, Revonsuo A, Pihko L, Portin R, Rinne JO. Visual object recognition deficits in early Parkinson's disease. *Parkinsonism Relat Disord*. 2004; 10: 227-233.
3. Possin KL, Filoteo JV, Song DD, Salmon DP. Spatial and object working memory deficits in Parkinson's disease are due to impairment in different underlying processes. *Neuropsychology*. 2008; 22: 585-595.
4. Siquier A, Andrés P. Episodic Memory Impairment in Parkinson's Disease: Disentangling the Role of Encoding and Retrieval. *J Int Neuropsychol Soc*. 2021; 27: 261-269.
5. Chung YC, Fisher BE, Finley JM, et al. Cognition and motor learning in a Parkinson's disease cohort: importance of recall in episodic memory. *Neuroreport.* 2021; 32: 1153-1160.
6. Solari N, Bonito-Oliva A, Fisone G, Brambilla R. Understanding cognitive deficits in Parkinson's disease: lessons from preclinical animal models. *Learn Mem*. 2013; 20: 592-600.
7. Sidransky E, Lopez G. The link between the GBA gene and parkinsonism. *Lancet Neurol.* 2012; 11: 986-987.
8. Goker-Alpan O, Schiffmann R, LaMarca ME, Nussbaum RL, McInerney-Leo A, Sidransky E. Parkinsonism among Gaucher disease carriers. *J Med Genet*. 2004; 41: 937-940.
9. Sidransky E, Nalls MA, Aasly JO, et al. Multicenter analysis of glucocerebrosidase mutations in Parkinson's disease. *N Engl J Med*. 2009; 361:1651-1661.
10. Brockmann K, Srulijes K, Hauser AK, et al. GBA-associated PD presents with nonmotor characteristics. *Neurology*. 2011; 77:276-280.
11. Alcalay RN, Caccappolo E, Mejia-Santana H, et al. Cognitive performance of GBA mutation carriers with early-onset PD: the CORE-PD study. *Neurology*. 2012; 78:1434-1440.
12. Zokaei N, McNeill A, Proukakis C, et al. Visual short-term memory deficits associated with GBA mutation and Parkinson's disease. *Brain*. 2014; 137, 2303-2311.

13. Goker-Alpan O, Stubblefield BK, Giasson BI, Sidransky E. Glucocerebrosidase is present in α-synuclein inclusions in Lewy body disorders. *Acta Neuropathol*. 12010; 20: 641-649.

14. Boyle PA, Yu L, Wilson RS, Schneider JA, Bennett DA. Relation of neuropathology with cognitive decline among older persons without dementia. *Front Aging Neurosci*. 2013; 5: 50.

15. Mazzulli JR, Xu YH, Sun Y, et al. Gaucher disease glucocerebrosidase and α-synuclein from a bidirectional pathogenic loop in synucleiopathies. *Cell*. 2011; 146: 37-52.

16. Taguchi YV, Liu J, Ruan J, et al. Glucosylsphingosine Promotes α-Synuclein Pathology in Mutant GBA-Associated Parkinson's Disease. *J Neurosci*. 2017; 37: 9617-9631.

17. Gegg ME, Burke D, Heales SJ, et al. Glucocerebrosidase deficiency in substantia nigra of parkinson disease brains. *Ann Neurol*. 2012; 72: 455-463.

18. Rocha EM, Smith GA, Park E, et al. Progressive decline of glucocerebrosidase in aging and Parkinson's disease. *Ann Clin Transl Neurol*. 2015; 2: 433-438.

19. Murphy KE, Gysbers AM, et al. Reduced glucocerebrosidase is associated with increased α-synuclein in sporadic Parkinson's disease. *Brain*. 2014; 137: 834-848.

20. Li H, Ham A, Ma TC, et al. Mitochondrial dysfunction associated with glucocerebrosidase deficiency l dysfunction and mitophagy defect triggered by heterozygous GBA mutations. Autophagy. *2019*; 15: 113-130.

21. Yun SP, Kim D, Kim S, et al. α-Synuclein accumulation and GBA deficiency due to L444P GBA mutation contributes to MPTP-induced parkinsonism. *Mol Neurodegener*. 2018; 13: 1.

22. Fishbein I, Kuo YM, Giasson BI, Nussbaum RL. Augmentation of phenotype in a transgenic Parkinson mouse heterozygous for a Gaucher mutation. *Brain*. 2014; 37: 3235-3247.

23. Migdalska-Richards A, Wegrzynowicz M, Rusconi R, et al. The L444P Gba1 mutation enhances alpha-synuclein induced loss of nigral dopaminergic neurons in mice. *Brain*. 2017; 140: 2706-2721.

24. Puzzo D, Lee L, Palmeri A, Calabrese G, Arancio O. Behavioral assays with mouse models of Alzheimer's disease: practical considerations and guidelines. *Biochem Pharmacol*. 2014; 88: 450-467.

25. Wu X, Sosunov AA, Lado W, et al. Synaptic hyperexcitability of cytomegalic pyramidal neurons contributes to epileptogenesis in tuberous sclerosis complex. *Cell Rep*. 2022; 40:111085.

26. Rockenstein E, Nuber S, Overk CR, et al. Accumulation of oligomer-prone α-synuclein exacerbates synaptic and neuronal degeneration in vivo. *Brain*. 2014; 137: 1496-1513.

27. Wirths O. Preparation of Crude Synaptosomal Fractions from Mouse Brains and Spinal Cords. *Bio Protoc*. 2017; 7: e2423.

28. Sardi SP, Clarke J, Kinnecom C, et al. CNS expression of glucocerebrosidase corrects alpha-synuclein pathology and memory in a mouse model of Gaucher-related synucleinopathy. *Proc Natl Acad Sci U S A*. 2011; 108: 12101-12106.

29. Clark LN, Chan R, Cheng R, et al. Gene-wise association of variants in four lysosomal storage disorder genes in neuropathologically confirmed Lewy body disease. *PLoS One*. 2015; 10: e0125204.

30. Surface M, Balwani M, Waters C, et al. Plasma Glucosylsphingosine in GBA1 Mutation Carriers with and without Parkinson's Disease. *Mov Disord*. 2022; 37: 416-421.

31. Chan RB, Oliveira TG, Cortes EP, et al. Comparative lipidomic analysis of mouse and human brain with Alzheimer disease. *J Biol Chem*. 2012; 287:2678-2688.

32. Mahoney-Crane CL, Viswanathan M, Russell D, et al. Neuronopathic GBA1L444P Mutation Accelerates Glucosylsphingosine Levels and Formation of Hippocampal Alpha-Synuclein Inclusions. *J Neurosci*. 2023; 43: 501-521.

33. Clarke JR, Cammarota M, Gruart A, Izquierdo I, Delgado-García JM. Plastic modifications induced by object recognition memory processing. *Proc Natl Acad Sci U S A*. 2010; 107: 2652-2657.

34. Nabavi S, Fox R, Proulx CD, Lin JY, Tsien RY, Malinow R. Engineering a memory with LTD and LTP. *Nature*. 2014; 511:348-352.

35. Abeliovich A, Schmitz Y, Fariñas I, et al. Mice lacking alpha-synuclein display functional deficits in the nigrostriatal dopamine system. *Neuron*. 2000; 25: 239-252.

36. Chesselet MF, Richter F, Zhu C, Magen I, Watson MB, Subramaniam SR. A progressive mouse model of Parkinson's disease: the Thy1- αSyn ("Line 61") mice. *Neurotherapeutics*. 2012; 9: 297-314.

37. Magen I, Fleming SM, Zhu C, et al. Cognitive deficits in a mouse model of pre-manifest Parkinson's disease. *Eur J Neurosci*. 2012; 35: 870-882.

38. Rockenstein E, Clarke J, Viel C, et al. Glucocerebrosidase modulates cognitive and motor activities in murine models of Parkinson's disease. *Hum Mol Genet*. 2016; 25: 2645-2660.

39. Richter F, Fleming SM, Watson M, et al. A GCase chaperone improves motor function in a mouse model of synucleinopathy. *Neurotherapeutics*. 2014; 11: 840-856.

40. Wu N, Joshi PR, Cepeda C, Masliah E, Levine MS. Alpha-synuclein overexpression in mice alters synaptic communication in the corticostriatal pathway. *J Neurosci Res*. 2010; 88: 1764-1876.

41. Nemani VM, Lu W, Berge V, et al. Increased expression of alpha-synuclein reduces neurotransmitter release by inhibiting synaptic vesicle reclustering after endocytosis. *Neuron*. 2010; 65: 66-79.

42. Anderson JP, Walker DE, Goldstein JM, et al. Phosphorylation of Ser-129 is the dominant pathological modification of alpha-synuclein in familial and sporadic Lewy body disease. J *Biol Chem*. 2006; 281: 29739-29752.

43. Rieker C, Dev KK, Lehnhoff K, et al. Neuropathology in mice expressing mouse alpha-synuclein. *PLoS One*. 2011; 6: e24834.

44. Soria FN, Engeln M, Martinez-Vicente M, et al. Glucocerebrosidase deficiency in dopaminergic neurons induces microglial activation without neurodegeneration. *Hum Mol Genet*. 2017; 26: 2603-2615.

45. McNeill A, Duran R, Proukakis C, et al. Hyposmia and cognitive impairment in Gaucher disease patients and carriers. *Mov Disord*. 2012; 27: 526-532.

46. Moran EE, Wang C, Katz M, et al. Cognitive and motor functioning in elderly glucocerebrosidase mutation carriers. *Neurobiol Aging*. 2017; 239.e1-239.e7.

47. Beavan M, McNeill A, Proukakis C, Hughes DA, Mehta A, Schapira AH. Evolution of prodromal clinical markers of Parkinson disease in a GBA mutation-positive cohort. *JAMA Neurol*. 2015; 72: 201-208.

48. Das T, Hwang JJ, Poston KL. Episodic recognition memory and the hippocampus in Parkinson's disease: A review. *Cortex*. 2019; 113: 191-209.

49. Brück A, Kurki T, Kaasinen V, Vahlberg T, Rinne JO. Hippocampal and prefrontal atrophy in patients with early non-demented Parkinson's disease is related to cognitive impairment. *J Neurol Neurosurg Psychiatry*. 2004; 75: 1467-1469.

50. Carlesimo GA, Piras F, Assogna F, Pontieri FE, Caltagirone C, Spalletta G. Hippocampal abnormalities and memory deficits in Parkinson disease:a multimodal imaging study. *Neurology*. 2012; 78: 1939-1845.

51. Kalaitzakis ME, Christian LM, Moran LB, Graeber MB, Pearce RK, Gentleman SM. Dementia and visual hallucinations associated with limbic pathology in Parkinson' disease. *Parkinsonism Relat Disord*. 2009; 15: 196-204.

52. Gegg ME, Sweet L, Wang BH, Shihabuddin LS, Sardi SP, Schapira AH. No evidence for substrate accumulation in Parkinson brains with GBA mutations. *Mov Disord*. 2015; 30: 1085-1089.

53. Tayebi N, Parisiadou L, Berhe B, et al. Glucocerebrosidase haploinsufficiency in A53T α-synuclein mice impacts disease onset and course. *Mol Genet Metab*. 2017; 122: 198-208.

54. Do J, Perez G, Berhe B, Tayebi N, Sidransky E. Behavioral Phenotyping in a Murine Model of *GBA1*-Associated Parkinson Disease. *Int J Mol Sci*. 2021; 22: 6826.

55. Giladi N, Alcalay RN, Cutter G, et al. Safety and efficacy of venglustat in GBA1-associated Parkinson's disease: an international, multicentre, double-blind, randomised, placebo-controlled, phase 2 trial. *Lancet Neurol*. 2023; 22: 661-671.

56. Fernandes HJ, Hartfield EM, Christian HC, et al. ER Stress and Autophagic Perturbations Lead to Elevated Extracellular α-Synuclein in GBA-N370S Parkinson's iPSC-Derived Dopamine Neurons. *Stem Cell Reports*. 2016; 6: 342-356.

57. Papadopoulos VE, Nikolopoulou G, Antoniadou I, et al. Modulation of β-glucocerebrosidase increases α-synuclein secretion and exosome release in mouse models of Parkinson's disease. *Hum Mol Genet*. 2018; 27: 1696-1710.

58. Baden P, Perez MJ, Raji H, et al. Glucocerebrosidase is imported into mitochondria and preserves complex I integrity and energy metabolism. *Nat Commun*. 2023; 14: 1930.

59. Guedes LC, Chan RB, Gomes MA, et al. Serum lipid alterations in GBA-associated Parkinson's disease. *Parkinsonism Relat Disord*. 2017; 44: 58-65.

60. Schverer M, O'Mahony SM, O'Riordan KJ, et al. Dietary phospholipids: Role in cognitive processes across the lifespan. *Neurosci Biobehav Rev*. 2020; 111: 183-193.

61. García-Sanz P, M F G Aerts J, Moratalla R. The Role of Cholesterol in α-Synuclein and Lewy Body Pathology in GBA1 Parkinson's Disease. *Mov Disord*. 2021; 36: 1070-1085.

62. Kiechle M, Grozdanov V, Danzer KM. The Role of Lipids in the Initiation of α-Synuclein Misfolding. *Front Cell Dev Biol*. 2020; 8: 562241.

63. Kim MJ, Jeon S, Burbulla LF, Krainc D. Acid ceramidase inhibition ameliorates α-synuclein accumulation upon loss of GBA1 function. Hum Mol Genet. 2018; 27: 1972-1988.

64. Blumenreich S, Nehushtan T, Barav OB, et al. Elevation of gangliosides in four brain regions from Parkinson's disease patients with a GBA mutation. *NPJ Parkinsons Dis*. 2022; 8: 99.

65. Huebecker M, Moloney EB, van der Spoel AC, et al. Reduced sphingolipid hydrolase activities, substrate accumulation and ganglioside decline in Parkinson's disease. *Mol Neurodegener*. 2019; 14: 40.

66. Chan RB, Perotte AJ, Zhou B, et al. Elevated GM3 plasma concentration in idiopathic Parkinson's disease: A lipidomic analysis. *PLoS One*. 2017; 12: e0172348.

67. Dodge JC, Tamsett TJ, Treleaven CM, et al. Glucosylceramide synthase inhibition reduces ganglioside GM3 accumulation, alleviates amyloid neuropathology, and stabilizes remote contextual memory in a mouse model of Alzheimer's disease. *Alzheimers Res Ther*. 2022; 14: 19.

68. Galvagnion C. The Role of Lipids Interacting with α-Synuclein in the Pathogenesis of Parkinson's Disease. *J Parkinsons Dis*. 2017; 7: 433-450.

69. Brekk OR, Honey JR, Lee S, Hallett PJ, Isacson O. Cell type-specific lipid storage changes in Parkinson's disease patient brains are recapitulated by experimental glycolipid disturbance. *Proc Natl Acad Sci U S A*. 2020; 117, 27646-27654.

Figure Legends

Figure 1 Cognitive and motor performance in 7-month-old *Gba1*$^{L444P/+}$ mice. (**A**) Contextual (Left) and Cued (Right) fear conditioning test. *Gba1*$^{L444P/+}$ (L444P, n=18) and WT control (CTRL, n=18) littermates show no differences in baseline (basal) freezing activities. During the contextual memory test, L444P mice show reduced freezing responses relative to their CTRL littermates. During the cued memory test, L444P and CTRL littermates spend similar time freezing; (**B**) L444P (n=12) and CTRL (n=12) littermates show no between-group difference in sensory perception of average foot shock intensities, at which the mice begin to show (1) first visible movement (e.g., flinching), (2) first gross motor movement (running or jumping), or (3) first audible response; (**C**) 2-day radial arm water maze (RAWM) working memory. Average number of errors committed during each three-trial training block of RAWM task is plotted. Compared to CTRL (n=19), L444P (n=16) mice show impaired working memory during test sessions on day 2; (**D, E**) Morris water maze (MMW) spatial learning (**D**) and probe test for reference memory (**E**) in CTRL (n=19) and L444P mice (n=18). The target quadrant #4 is indicated by the red square; (**F, G**) The average escape latency (**F**) and swimming speed (**G**) during a visible platform water maze task. CTRL (n=15) and L444P (n=15) mice show similar time to reach the visible platform and similar velocity of swimming; (**H**) Novel object recognition memory. Compared to CTRL (n=17), L444P mice (n=18) spend less time sniffing the novel object, with a reduced discrimination index for novel object preference (0.69 ± 0.01 in CTRL v.s. 0.52 ± 0.01 in L444P mice); (**I**) Accelerating rotarod performance. Compared to CTRL (n=20), L444P mice (n=20) show no difference in average latency to fall from the rotarod during each session; (**J**) Balance beam performance. There are no differences between CTRL (n=18) and L444P mice (n=18) in time to transverse the beam; (**K**) Open field performance. CTRL (n=16) and L444P (n=16) littermates show no differences in the percentage of time spent in the center compartment, average total distance traveled, and number of rearing events (vertical counts). For all tests, similar number

of male and female mice are used. All data are mean ± SEM. *, p<0.05; **, p<0.01; ***, p<0.001. two-tailed unpaired t test (**G, J, K**) or two-way ANOVA followed by the Fisher's Least Significant Difference (LSD) test (**A, B, C, D, E, F, H** and **I**). Source data are provided in **Supplementary Table 1**.

Figure 2 Synapse pathology in *Gba1*$^{L444P/+}$ mice at 2.5 months of age. (**A**) Theta burst stimulation (TBS) evoked LTP in control (CTRL) and *Gba1*$^{L444P/+}$ (L444P) mice. For each genotype, n = 7 slices from 6 animals, 3 males and 3 females. Data are mean ± SEM. **, p<0.01, two-tailed unpaired t test; (**B**) Representative current traces of mEPSCs (upper) and the quantification of mEPSC frequency and amplitude (lower). Compared to CTRL, L444P mice show reduced mEPSC frequency. For each genotype, n= 14-15 neurons from 3 males and 3 females. Data are mean ± SEM. **, p<0.01, two-tailed unpaired t test; (**C**) EPSC responses (mean ± SEM) in CA1 neurons to paired pulse stimulation of Schaffer collaterals with a 50 ms interstimulus interval (ISI). L444P mice do not show changes in paired-pulse ratio. Two-tailed Mann-Whitney test. n = 14 (CTRL) or 11 (L444P) neurons from 2 males and 3 females; (**D**) DiOlistic labeling of mouse hippocampus. Blue: DAPI; Yellow: DiI. On the right shows CA1 pyramidal neurons from both genotypes. Compared to CTRL, L444P mice show a reduction in the number of primary basal dendrites. 20 neurons from 3-4 mice per genotype. Scale: 200 μm (Left) and 20 μm (Right). Data are mean ± SEM. *, p<0.05, two-tailed Mann-Whitney test; (**E**) Apical and basal dendritic segments from CA1 pyramidal neurons of CTRL and L444P mice. Mature spines were defined as dendritic protrusions with the ratio of head/neck diameter >1.1 (see methods). Three dendritic segments per neuron, 20 neurons from 4 mice per condition. Compared to CTRL, L444P mice show a reduction in mature spines in both apical and basal dendrites. Scale: 5μm. Data are mean ± SEM. ***, p<0.001, two-tailed unpaired t test; (**F**) Western blot analysis of αSyn, GCase, NeuN, presynaptic proteins synapsin I (SYN1) and synaptophysin (SYP), and postsynaptic protein PSD95 in the hippocampus of CTRL (n=8) and L444P (n=8) mice. Protein levels are normalized to actin and expressed as % of the mean of CTRL (CTRL mean). Data are mean ± SEM. ***, p<0.001, two-tailed unpaired t test. Source data are provided in **Supplementary Table 2**.

Figure 3 Downregulating αSyn levels does not mitigate cognitive impairment associated with *GBA1* mutation. (**A**) Western blot analysis of αSyn from CTRL, *Gba1*$^{L444P/+}$ (L444P), *Snca*+/-, *Snca*KO, L444P: *Snca*+/- and L444P:*Snca*KO mice at 2.5 months. n= 4 mice per genotype. Protein levels are normalized to actin and expressed as % of CTRL mean. Data are mean ± SEM. ***, p<0.001; ns, non-significant. One-way ANOVA followed by Tukey's multiple comparison test; (**B-G**) Cognitive and motor functions in CTRL, L444P, *Snca*+/-, *Snca*KO, L444P:*Snca*+/- and L444P:*Snca*KO mice at 2.5 months of age. (**B, C**) Contextual (**B**) and cued (**C**) feared memory. n = 10-11 animals per genotype, with approximately equal numbers of males and females. There are no differences in contextual and cued fear memories between CTRL, *Snca*+/- and *Snca*KO mice. The presence of L444P/+ mutation impairs contextual memory in L444P, L444P:*Snca*+/- and L444P:*Snca*KO mice. Data are mean ± SEM. **, p<0.01; ns, non-significant. Two-way ANOVA followed by Tukey's multiple comparison test; (**D, E**) Morris water maze (MMW) spatial learning (**D**) and spatial memory (**E**). n = 10-11 animals per genotype, with approximately equal numbers of males and females. *Snca*+/- and *Snca*KO mice show normal MMW spatial learning and memory, whereas the presence of L444P mutation impairs spatial memory in L444P, L444P:*Snca*+/- and L444P:*Snca*KO mice. Data are mean ± SEM. **, p<0.01; ns, non-significant. Two-way ANOVA followed by Tukey's multiple comparison test; (**F**) Accelerating rotarod performance (mean ± SEM) showing no between-group differences. n = 10-14 animals per genotype, with approximately equal numbers of males and females. Two-way ANOVA followed by Tukey's multiple comparison test; (**G**) Open field behaviors showing no between-group differences. N=10-14 animals per genotype, with approximately equal numbers of males and females. Data are mean ± SEM, One-way ANOVA; (**H**) mEPSC frequency and amplitude in CTRL, L444P, *Snca*KO and L444P:*Snca*KO mice at 2.5 months of age. Compared to CTRL, *Snca*KO mice show no changes in mEPSC frequency or amplitude, whereas L444P and L444P:*Snca*KO mice show reduced mEPSC frequency. For each genotype, n = 10-12 neurons from 5-6 mice. Data are mean ± SEM. *, p<0.05; **, p<0.01; ***, p<0.001. One-way ANOVA followed by Tukey's multiple comparison test; (**I**) Paired pulse facilitation of EPSCs in hippocampal CA3-CA1 synapses in CTRL, L444P, *Snca*KO and L444P:*Snca*KO mice at 2.5 months of age. For each genotype, n=13-17 neurons from 5-7 mice. There are no between-group differences in paired pulse ratio (PPR, mean ± SEM), one-way ANOVA followed by Tukey's multiple comparison test. Source data are provided in **Supplementary Table 3**.

Figure 4 Altered lipid profile in the *Gba1*$^{L444P/+}$ mouse hippocampus. (**A, B**) Reduced GCase enzyme activity in *Gba1*$^{L444P/+}$ (L444P) hippocampus at 2.5 (**A**) and 7 (**B**) months of age. Data are mean ± SEM, n=4 mice per genotype. **, p<0.01; ***, p<0.001. Two-tailed unpaired t test; (**C, D**) GCase substrates GluCer and GluSph in L444P hippocampus at 2.5 (**C**) and 7 (**D**) months of age. For each condition, n = 4 mice. Data are mean ± SEM. *, p<0.05, two-tailed unpaired t test; (**E, F**) Lipidomic analysis in CTRL and L444P mouse hippocampus at 2.5 (**E**) and 7 (**F**) months of age. For each condition, n = 3 mice. At 7 months, L444P mice show an increase in GM3 and CE, but a decrease in phospholipid classes including PA, PE, PS, PI, BMP, LPC and LPS, and sphingolipid species Ceramide (Cer), Sphingomyelin (SM). Data are mean ± SEM. *, p<0.05; **, p<0.01; ***, p<0.001. Two-tailed unpaired t test. Source data are provided in **Supplementary Table 4**.

Figure 5 L444P/+ *Gba1* mutation exacerbates cognitive and synaptic impairment associated with αSyn accumulation at 2.5 months of age. (**A**-**E**) Behavioral characterization of *Gba1*$^{L444P/+}$ (L444P), Thy1-αSyn (ASO) and *Gba1*$^{L444P/+}$:Thy1-αSyn (L444P:ASO) double mutant mice at 2.5 months. (**A**) Contextual (Left) and cued fear memory (Right). n = 13-22 animals per genotype; (**B-C**) MWM spatial learning (**B**) and memory (**C**). n = 14-16 animals per genotype; (**D**) Accelerating rotarod performance. n = 10-13 animals per genotype; (**E**) Open field performance. n = 10-19 animals per genotype. Data are mean ± SEM. *, p<0.05; **, p<0.01; ***, p<0.001. One-way ANOVA followed by Tukey's multiple comparison test; (**F**) Theta-burst induced hippocampal CA3-CA1 LTP in CTRL, L444P, ASO and L444P:ASO mice at 2.5 months. n=10-12 slices per genotype. Data are mean ± SEM. **, p<0.01; ***, p<0.001; ns, non-significant. One-way ANOVA followed by Tukey's multiple comparison test; (**G**) Frequency and amplitude of mEPSC in hippocampal CA1 neurons from CTRL, L444P, ASO and L444P:ASO mice at 2.5 months. Both L444P and ASO mice show reduced frequency but no changes in amplitude, and the double mutant mice display a further reduction in mEPSC frequency. n= 10-13 neurons per genotype. Data are mean ± SEM. *, p<0.05; ***, p<0.001; ns, non-significant. One-way ANOVA followed by Tukey's multiple comparison test; (**H**) Paired pulse ratio (PPR) in hippocampal CA3-CA1 synapses of CTRL, L444P, ASO and L444P:ASO mice at 2.5 months. Compared to CTRL, ASO

and L444P:ASO mice show an increase in PPR. n= 11-22 neurons per genotype. Data are mean ± SEM. *, p<0.05; **, p<0.01. One-way ANOVA followed by Tukey's multiple comparison test; (**I**) NMDAR- and AMPAR components of evoked EPSCs in CA1 pyramidal neurons. n=10-14 neurons per genotype. Data are mean ± SEM. One-way ANOVA followed by Tukey's multiple comparison test. Source data are provided in **Supplementary Table 5**.

Figure 6 L444P/+ *Gba1* mutation exacerbates synaptic αSyn accumulation in Thy1-αSyn mice at 2.5 months of age. (**A**) Western blot analysis of GCase, αSyn, p- αSyn and synaptic proteins (SYN1, PSD95) in the hippocampus of control (CTRL), *Gba1*$^{L444P/+}$ (L444P), Thy1-αSyn (ASO) and *Gba1*$^{L444P/+}$:Thy1-αSyn (L444P:ASO) double mutant mice at 2.5 months of age. Protein levels are normalized to actin and expressed as % of CTRL mean. Data are mean ± SEM. **, p<0.01; ***, p<0.001. One-way ANOVA followed by Tukey's multiple comparison test. n=4 mice per genotype; (**B**) Immunohistochemistry of αSyn and Ser129 p-αSyn in the hippocampus of CTRL, L444P, ASO, L444P:ASO mice at 2.5 months of age. Micrographs are representative of three independent experiments. Scale: 200μm. As in Rockenstein et al (2014), [26] αSyn and p-αSyn accumulate in both neuronal cell body and neuropil in ASO mice. L444P:ASO mice show highest levels of αSyn and p-αSyn among all four mouse lines; (**C**) Co-immunostaining of αSyn and presynaptic marker synaptophysin (SYP) in the hippocampus of Thy1-αSyn (ASO) mice. Scale: 10μm. Blue, DAPI stain for nucleus; (**D**) Levels of CA1 Striatum radiatum αSyn in CTRL, L444P, ASO and L444P:ASO mice at 2.5 months of age. Scale: 10μm. *Snca*KO mice are used as negative controls. Micrographs are representative of three independent experiments; (**E**) Synaptosome fractionation from CTRL mice. Total hippocampal lysates, nucleus, cytosolic and synaptosome (SPM) fractions were subjected to Western blot analysis for presynaptic protein synapsin 1 (SYN1), postsynaptic proteins PSD95 and GluR1, nuclear protein marker Lamin B and cytosolic protein marker GAPDH. The SPM fraction is enriched for synaptic proteins SYN1, PSD95 and GluR1 but absent for Lamin B and GAPDH; **(F)** Western blot analysis of αSyn and p-αSyn in synaptosomes (SPM) fractionated from CTRL, L444P, ASO and L444P:ASO mice at 2.5 months of age. SPM fraction from *Snca*KO mice is used as a negative control; (**G-H)** Quantification of synaptosomal αSyn (**G**) and p-αSyn (**H**) in CTRL, L444P, ASO and L444P:ASO mice. For each genotype, n=3 animals. Protein levels are normalized to PSD95 and expressed as % of CTRL mean in (**G**) and % of ASO mean in (**H**). Compared to CTRL, L444P mice show

increased synaptic levels of αSyn but not p- αSyn. Both ASO and L444P:ASO mice have higher levels of synaptic αSyn and p-αSyn than CTRL and L444P mice. When compared to ASO littermates, L444P:ASO mice present a further accumulation of synaptic αSyn and p- αSyn. Data are mean ± SEM. *, p<0.05; **, p<0.01; ***, p<0.001; ns, non-significant. One-way ANOVA followed by Tukey's multiple comparison test; (**I, J**) GCase enzyme activity (**I**) and levels of GCase substrates GluCer and GluSph (**J**) in CTRL, L444P, ASO and L444P:ASO mice at 2.5 months of age. n=4 mice per genotype. Data are mean ± SEM. **, p<0.01; ***, p<0.001. One-way ANOVA followed by Tukey's multiple comparison test. Source data are provided in **Supplementary Table 6**.

Figure 7 L444P/+ *Gba1* mutation exacerbates synaptic and motor impairment associated with αSyn accumulation at 7 months of age. (**A-E**) Behavioral characterization of Control (CTRL), *Gba1*$^{L444P/+}$ (L444P), Thy1-αSyn (ASO) and *Gba1*$^{L444P/+}$:Thy1-αSyn double mutant (L444P:ASO) mice at 7 months of age. (**A**) Contextual (Left) and cued fear memory (Right); (**B**) MWM spatial learning; (**C**) MWM spatial memory; (**D**) Open field performance; (**E**) Accelerating rotarod performance. CTRL, n=10-19; L444P, n=10-19; ASO, n=10-12; L444P:ASO double mutants, n = 10-13. Data are mean ± SEM. *, p<0.05; **, p<0.01; ***, p<0.001; ns, non-significant. One-way ANOVA followed by Tukey's multiple comparison test; (**F**) Theta-burst induced LTP in four mouse lines at 7 months of age. n=10 slices per genotype from 5-7 mice. Data are mean ± SEM. *, p<0.05; **, p<0.01; ns, non-significant. One-way ANOVA followed by Tukey's multiple comparison test; (**G**) Western blot analysis of GCase, αSyn, p-αSyn, NeuN, and synaptic proteins (SYN1, PSD95) in the hippocampus of CTRL, L444P, ASO and L444P:ASO mice at 7 months of age. n=4 mice per genotype. Data are mean ± SEM. *, p<0.05; **, p<0.01; ***, p<0.001; ns, non-significant. One-way ANOVA followed by Tukey's multiple comparison test; (**H, I**) GCase enzyme activity (**H**) and levels of GCase substrates GluCer and GluSph (**I**) in CTRL, L444P, ASO and L444P:ASO mice at 7 months of age. n=4 mice per genotype. Data are mean ± SEM. **, p<0.01; ***, p<0.001. One-way ANOVA followed by Tukey's multiple comparison test. Source data are provided in **Supplementary Table 7**.

Figure 8 Cognitive function in dopaminergic neuronal specific *Gba1* deficient mice at 2.5 month of age. (**A**) Levels of dopamine (DA) and its metabolite dihydroxyphenylacetic acid (DOPAC) in different brain regions (striatum, midbrain, hippocampus and frontal cortex) of control (CTRL), *Gba1*$^{L444P/+}$ (L444P), Thy1-αSyn (ASO) and *Gba1* $^{L444P/+}$:Thy1-αSyn double mutant (L444P:ASO) mice at 2.5 months of age**.** The amount of DA and DOPAC is calculated and normalized to protein concentration. For each genotype, n= 6 animals. Data are mean ± SEM. One-way ANOVA followed by Tukey's multiple comparison test; (**B-H**) Cognitive and motor function in control and dopaminergic neuronal specific *Gba1*CKO mice at 2.5 month of age. DAT-Cre (CTRL), n=9; *Gba1*$^{flox/+}$:DAT-Cre+ heterozygous (*Gba1*het) mice, n=9; homozygous *Gba1*$^{flox/flox}$:DAT-Cre+ (*Gba1*CKO) mice, n=13; (**B, C**) Contextual (**B**) and cued (**C**) fear memory; (**D, E**) Morris water maze learning (**D**) and memory (**E**); (**F**) Accelerating rotarod performance; (**G**) Balance beam motor coordination; (**H**) Open field behaviors. Compared to CTRL littermates, *Gba1*Het and *Gba1*CKO mice show normal cognitive and motor behaviors. Data are mean ± SEM. One-way ANOVA followed by Tukey's multiple comparison test. Source data are provided in **Supplementary Table 8**.

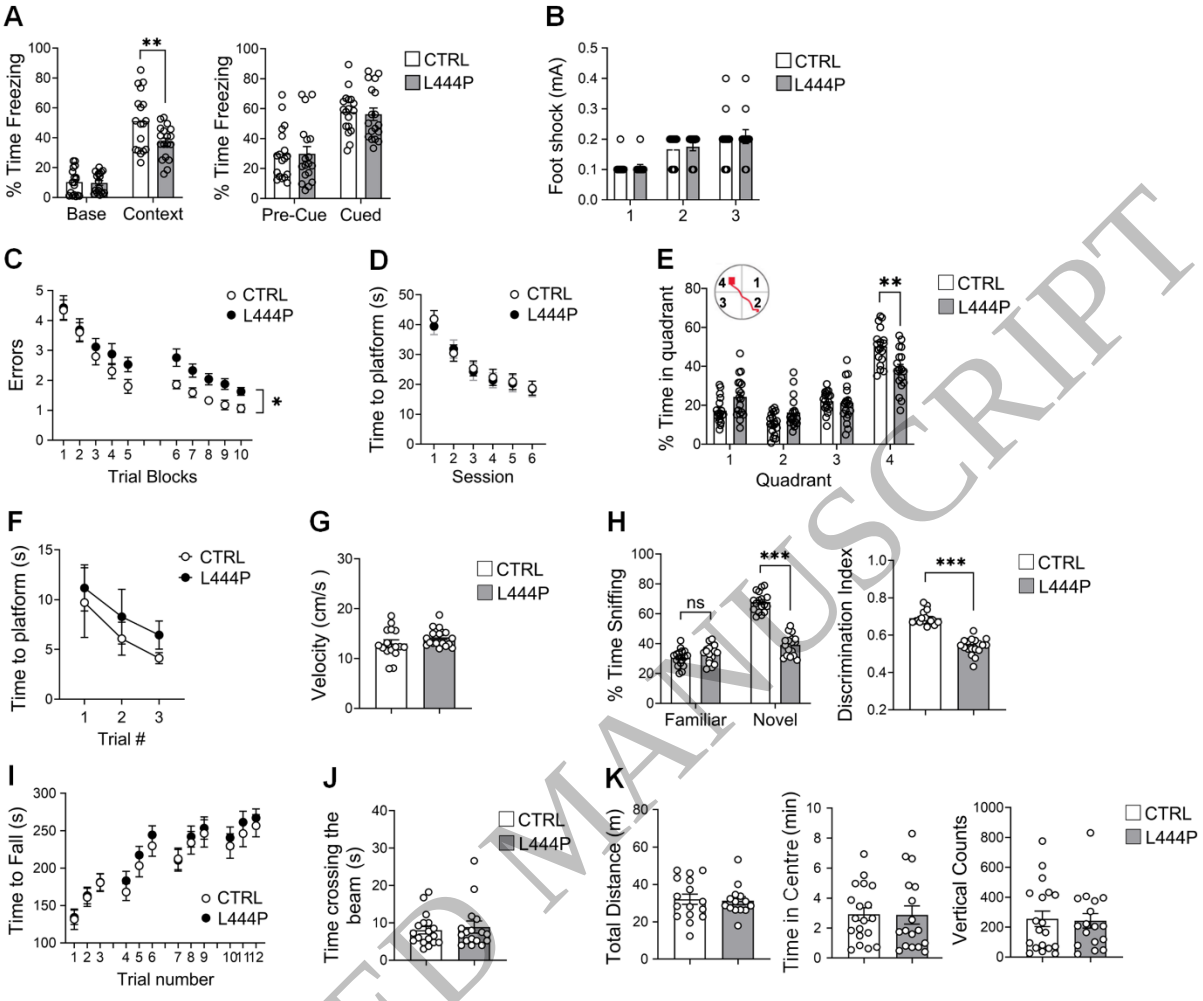

Figure 1
165x132 mm (x DPI)

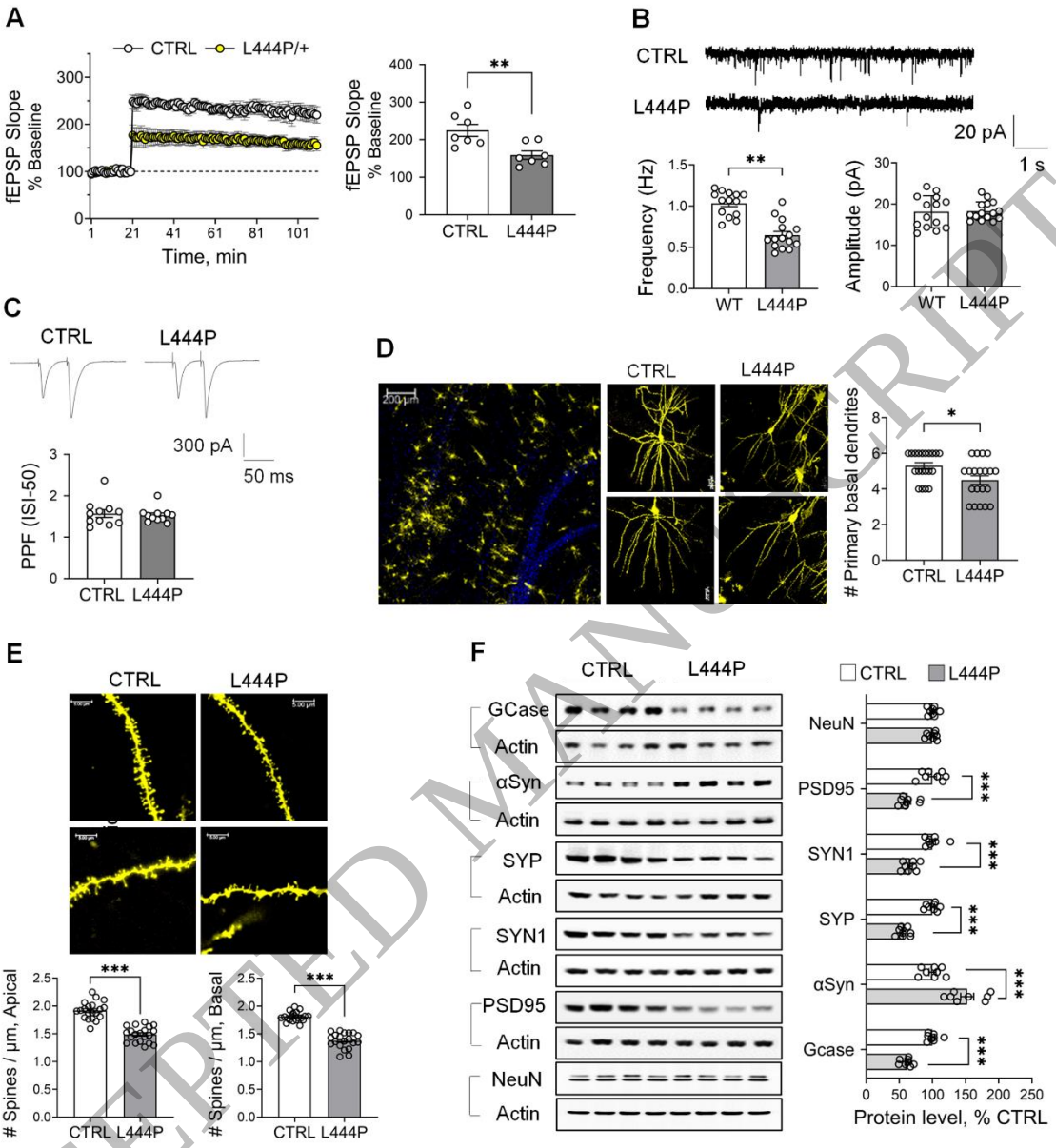

Figure 2
150x163 mm (x DPI)

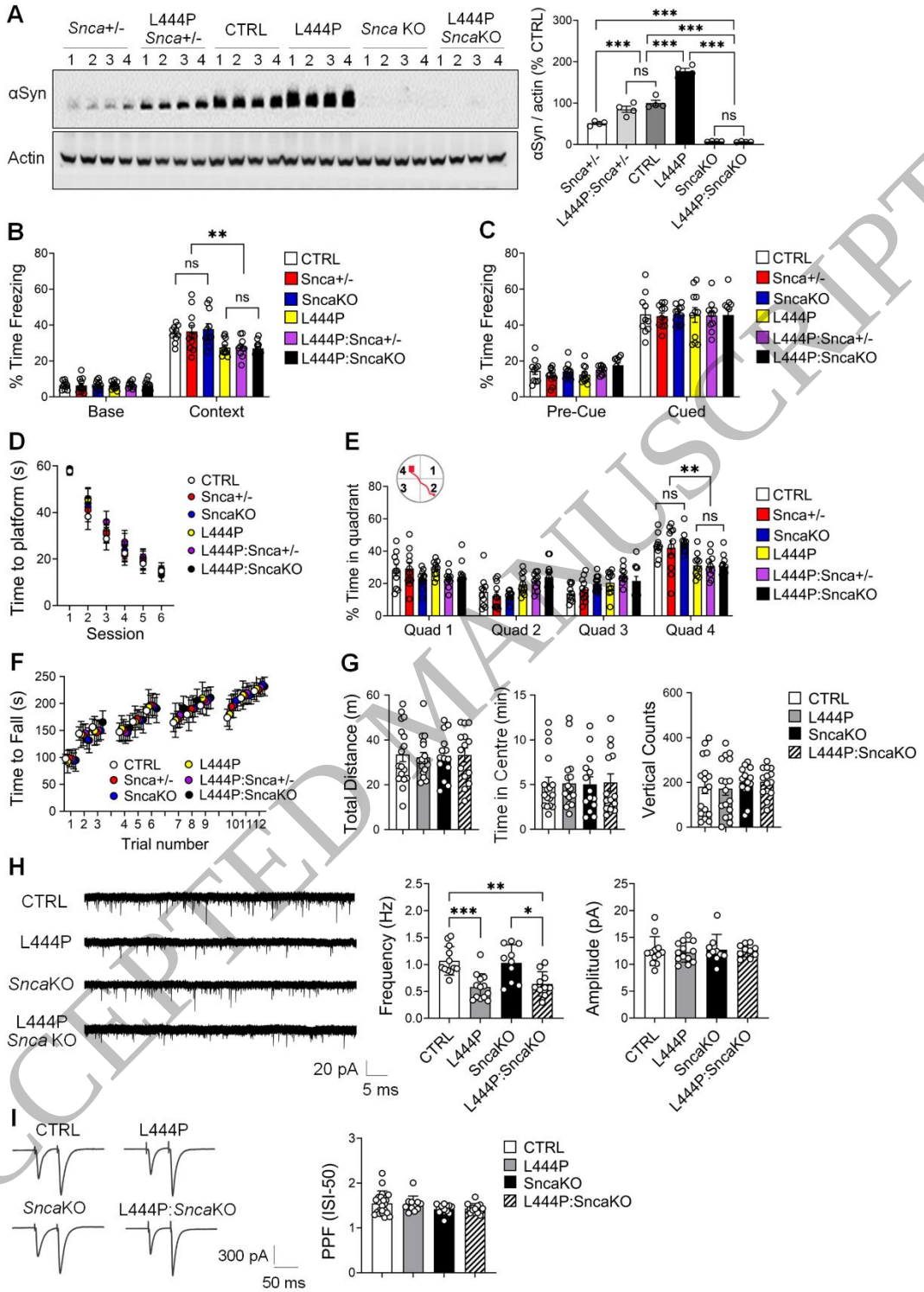

Figure 3
144x201 mm (x DPI)

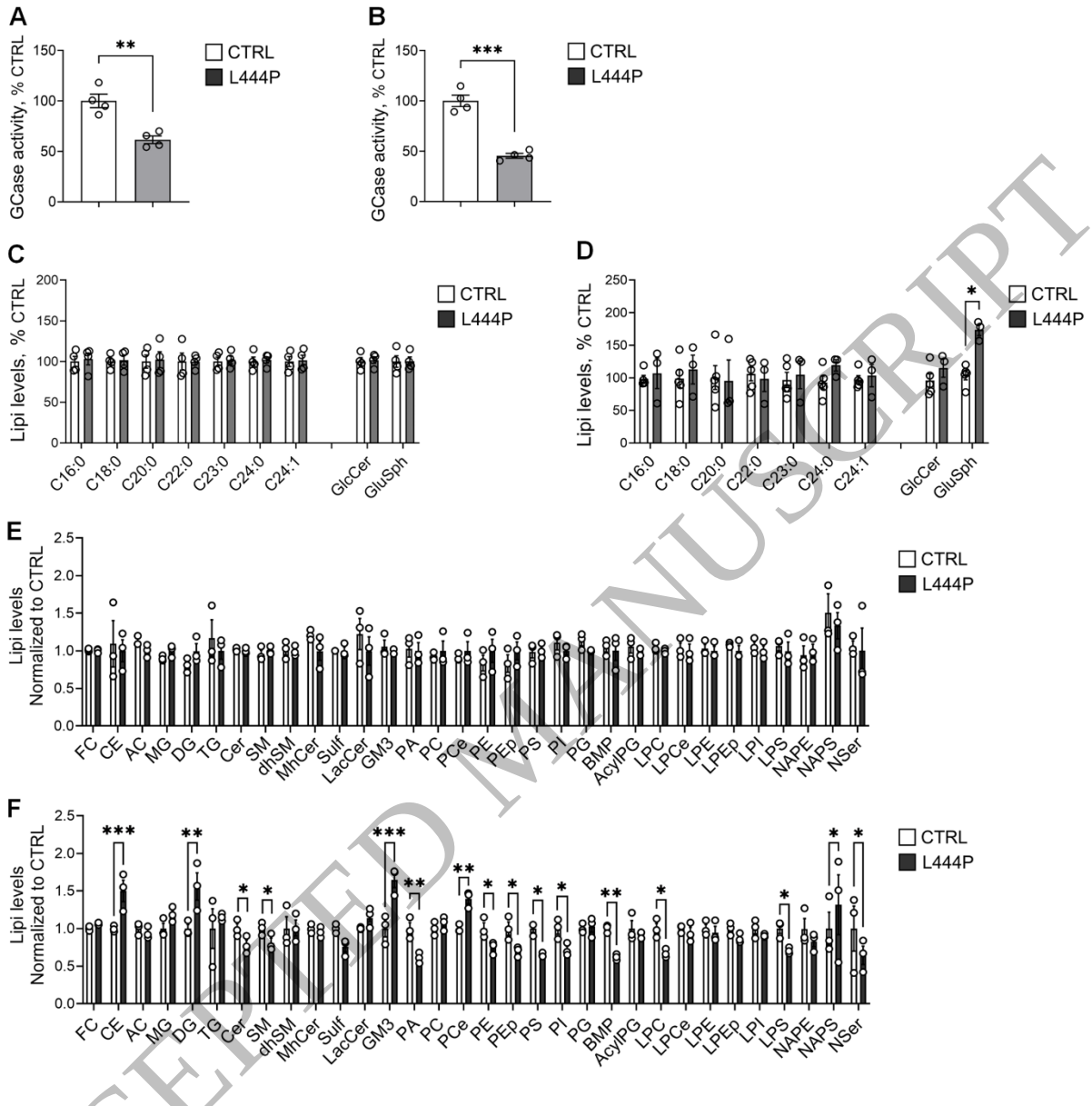

Figure 4
165x160 mm (x DPI)

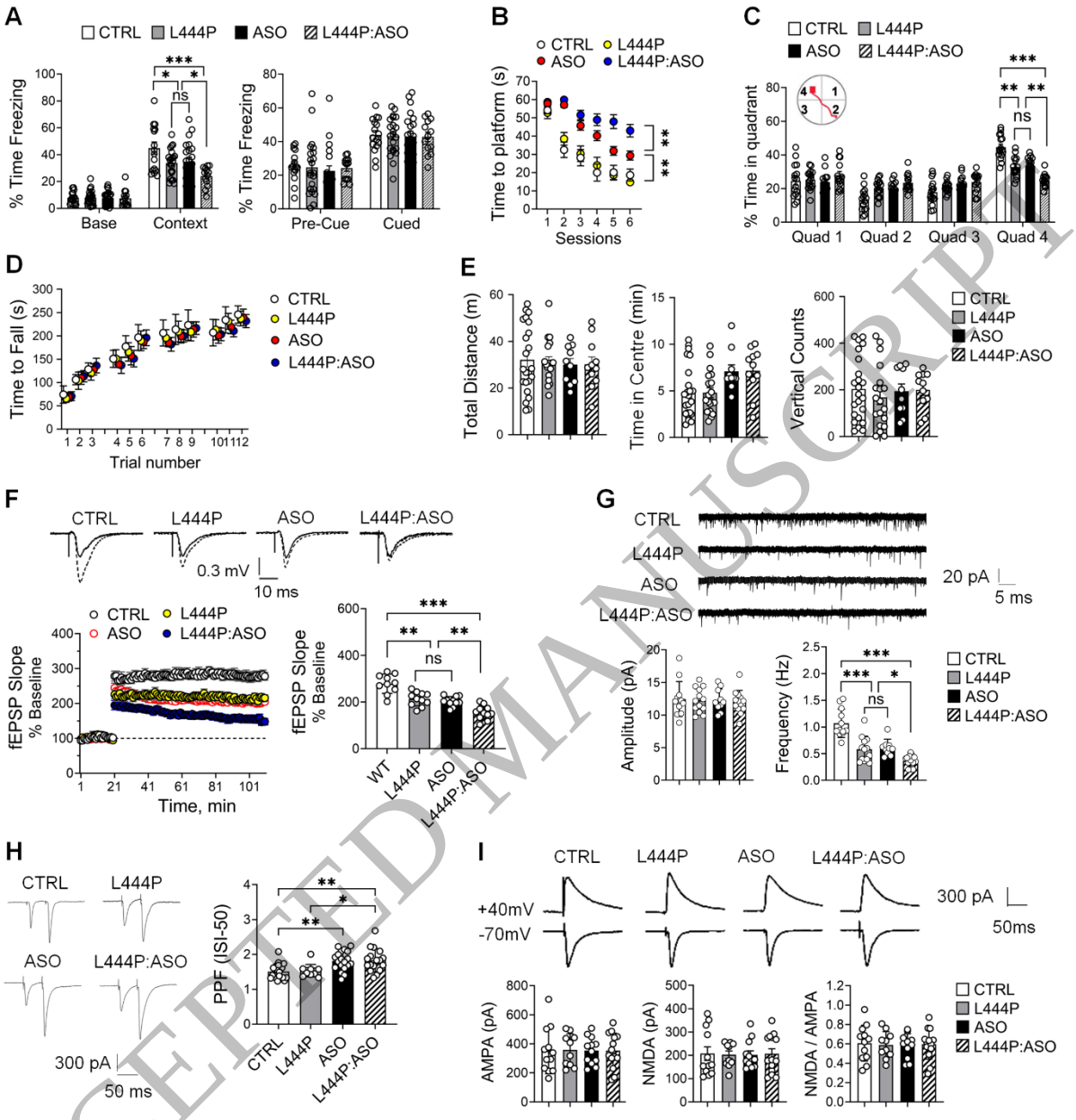

Figure 5
165x166 mm (x DPI)

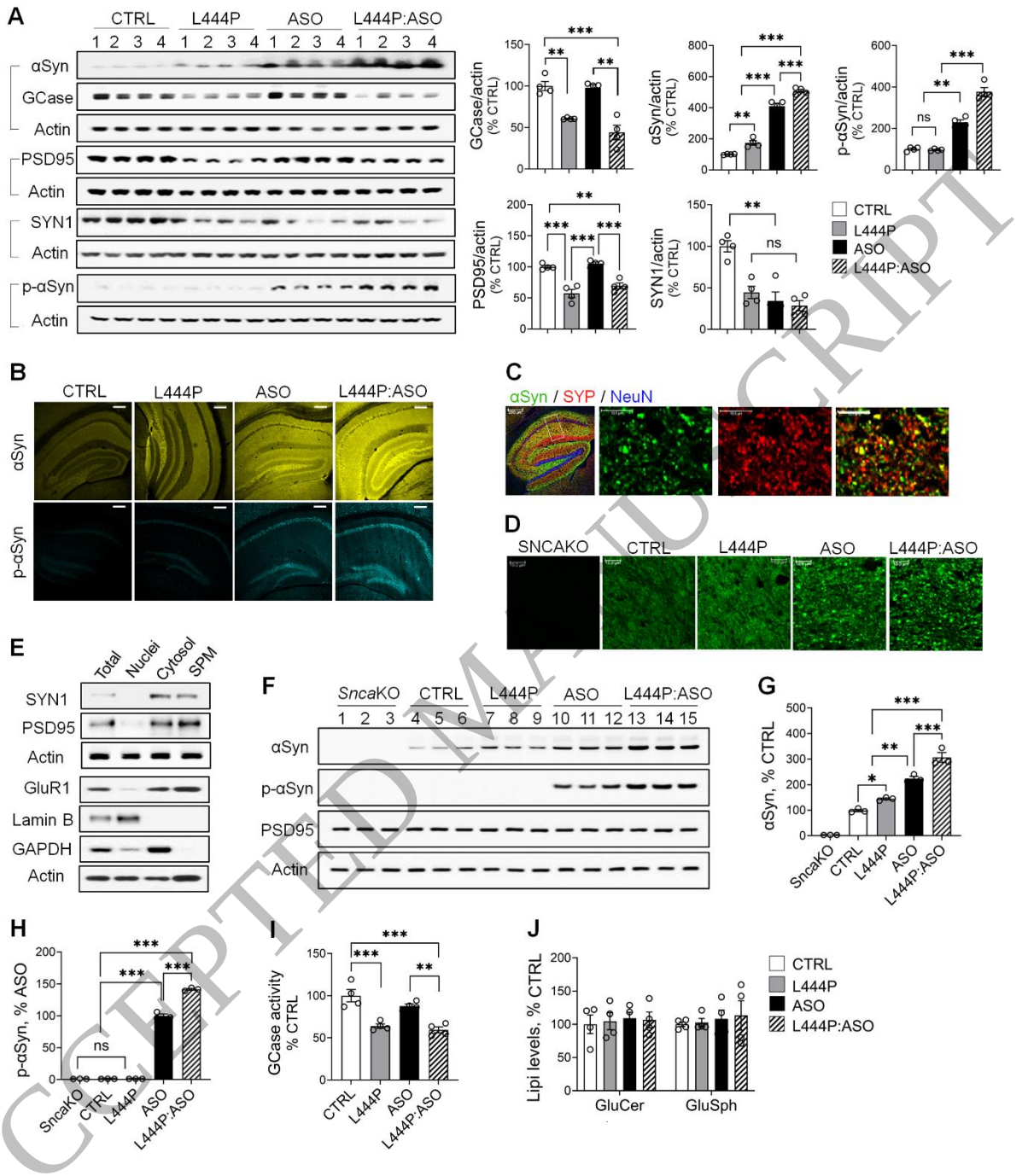

Figure 6
165x181 mm (x DPI)

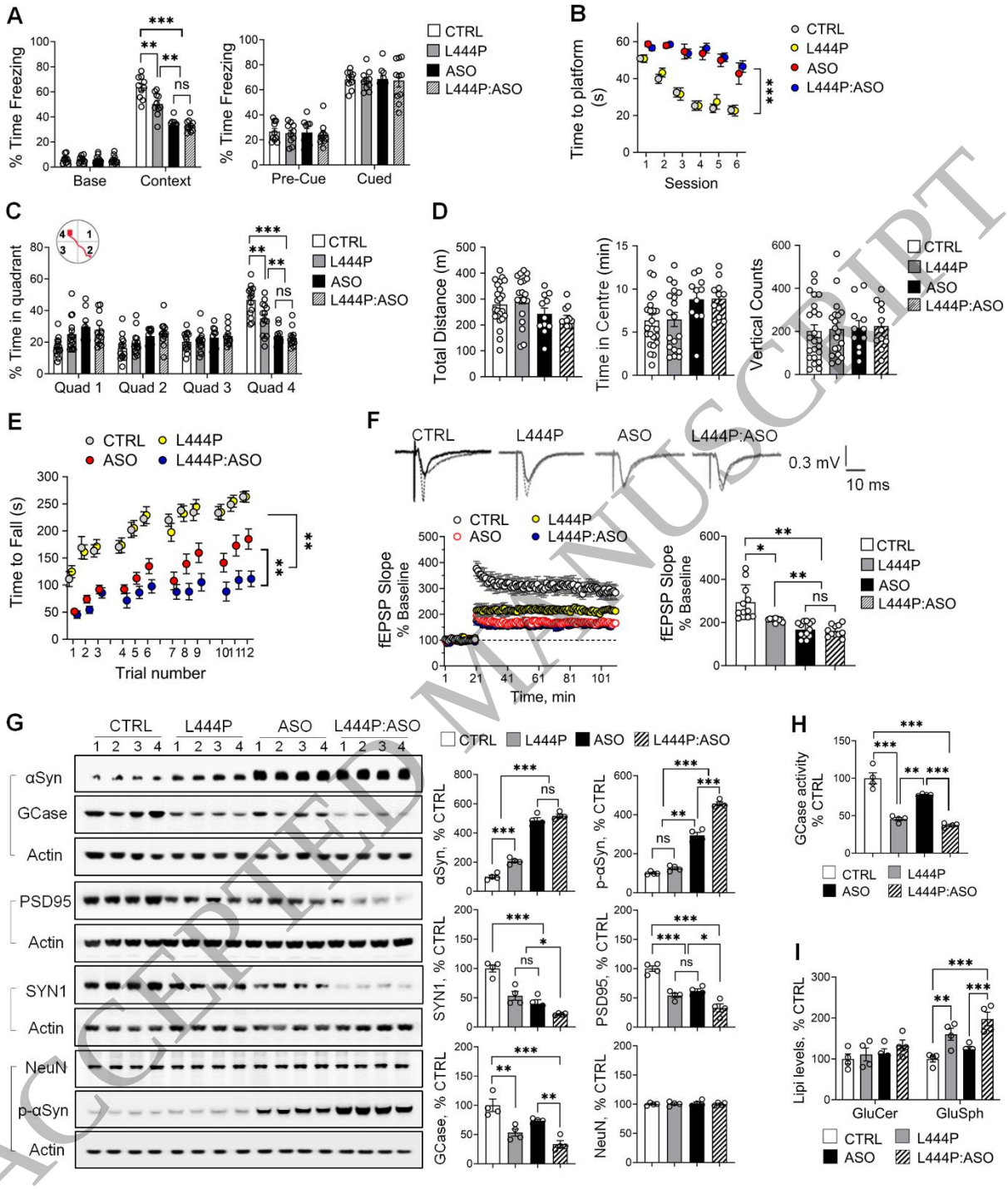

Figure 7
165x189 mm (x DPI)

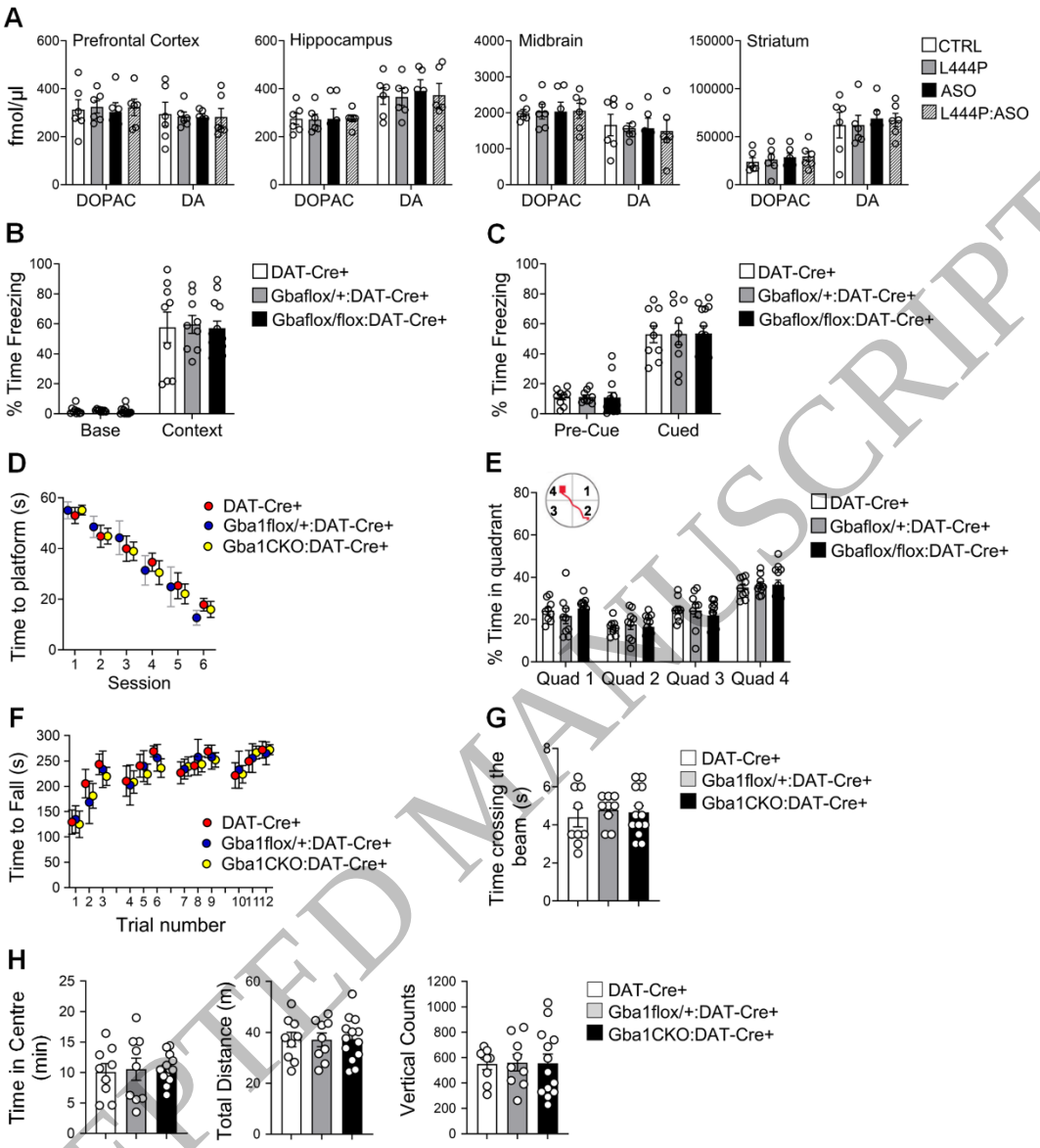

Figure 8
142x159 mm (x DPI)